Oceanic Regime Shift to a Warmer Continental Shelf Adjacent to the Shackleton Ice Shelf, East Antarctica

Natalia Ribeiro, Laura Herraiz-Borreguero, Stephen R Rintoul, Guy Williams, Clive R Mcmahon, Mark Hindell, Christophe Guinet

JGR Oceans

RESEARCH ARTICLE
10.1029/2023JC019882

Oceanic Regime Shift to a Warmer Continental Shelf Adjacent to the Shackleton Ice Shelf, East Antarctica

Natalia Ribeiro[1], Laura Herraiz-Borreguero[2,3], Stephen R. Rintoul[2,3], Guy Williams[4,5], Clive R. McMahon[6], Mark Hindell[1], and Christophe Guinet[7]

[1]Institute for Marine and Antarctic Studies, University of Tasmania, Hobart, TAS, Australia, [2]Commonwealth Scientific and Industrial Research Organization Environment (CSIRO), Hobart, TAS, Australia, [3]Australian Antarctic Program Partnership, University of Tasmania, Hobart, TAS, Australia, [4]First Institute of Oceanography, Qingdao, China, [5]Ocean University of China, Qingdao, China, [6]IMOS Animal Tagging, Sydney Institute of Marine Science, Mosman, NSW, Australia, [7]Centre d'Etudes Biologiques de Chizé, UMR 7372 CNRS-La Rochelle Université, Villiers en Bois, France

Abstract The long-held view that the East Antarctic margin is isolated from warm offshore waters has been challenged by recent observations showing incursions of warm modified Circumpolar Deep Water (mCDW) reaching several East Antarctic ice shelves. However, large areas of the East Antarctic continental shelf remain poorly observed, making it challenging to determine if the supply of oceanic heat to the ice shelves is changing. Here, we use temperature and salinity profiles to the west of the Shackleton Ice Shelf (SIS; ≈100°E) spanning 60 years to assess the variability of the water masses in the context of a changing climate. We document warming and freshening of shelf waters. Prior to 1996, cold mCDW water ($\theta < -1.6$°C) was found below the surface mixed layer and cold Dense Shelf Water (DSW) with a salinity of >34.5 dominated the water column. After 2010, warm mCDW (≥−1.0°C) was widespread over the continental shelf and DSW with salinity over 34.5 was no longer present. The mixing ratio of glacial meltwater indicates that warm mCDW observed in 2011 caused basal melting of the SIS, possibly reducing the salinity of DSW. Increased access of warm waters to the continental shelf may have also occurred on the eastern side of the ice shelf, where glaciological evidence shows the grounding line has retreated. These observations suggest a shift occurred prior to 2011 that has increased the ocean heat supply to the continental shelf and to the SIS, increasing basal melt and reducing DSW formation.

Plain Language Summary Recently, relatively warm waters that are normally found offshore are coming onto the Antarctic continental shelves, threatening the stability of East Antarctic ice shelves. The process, known as an "intrusion," is mostly reported in West Antarctica. Yet, recent studies have documented similar warm water intrusions in East Antarctica. East Antarctica contains more ice mass than West Antarctica and thus, its potential contributions to sea level rise are also higher. It is not known if these intrusions have always happened, or if they started at a particular point in time. Much less is known about what mechanisms make them happen. This study shows warm water intrusions reach the Shackleton Ice Shelf from 2011 onwards. The intrusions melt the ice shelf from below and the freshwater resulting from this melt goes into the ocean and freshens it. It also increases the stratification of the water column, making it harder for polynyas, massive open ocean areas that form next to the Antarctic margins during the Austral winter, to produce an important dense water variety that supplies the bottom layer of the world ocean's circulation.

Key Points:

- Ocean observations spanning 60 years document a shift in shelf water properties west of the Shackleton Ice Shelf (SIS)
- Pre-1996, modified Circumpolar Deep Water (mCDW) warmer than −1.6°C was not observed; post-2010, warm mCDW (≥−1°C) was widespread to the west of the SIS
- The observed mCDW intrusions cause basal melt of the SIS, freshening Dense Shelf Water and hindering its production

Supporting Information:

Supporting Information may be found in the online version of this article.

Correspondence to:

N. Ribeiro,
natalia.ribeirosantos@utas.edu.au

Citation:

Ribeiro, N., Herraiz-Borreguero, L., Rintoul, S. R., Williams, G., McMahon, C. R., Hindell, M., & Guinet, C. (2023). Oceanic regime shift to a warmer continental shelf adjacent to the Shackleton Ice Shelf, East Antarctica. *Journal of Geophysical Research: Oceans*, *128*, e2023JC019882. https://doi.org/10.1029/2023JC019882

Received 1 APR 2023
Accepted 5 OCT 2023

Author Contributions:

Conceptualization: Natalia Ribeiro, Laura Herraiz-Borreguero, Stephen R. Rintoul, Guy Williams
Data curation: Natalia Ribeiro, Laura Herraiz-Borreguero, Clive R. McMahon, Mark Hindell, Christophe Guinet
Formal analysis: Natalia Ribeiro
Funding acquisition: Laura Herraiz-Borreguero, Stephen R. Rintoul, Guy Williams, Clive R. McMahon, Mark Hindell, Christophe Guinet

1. Introduction

The East Antarctic Ice Sheet (EAIS) has historically been considered to be more stable than its counterpart in West Antarctica. This is so because much of the ice sheet was believed to rest on bedrock elevated above sea level and because the marine-based sectors were believed to be isolated from warm ocean waters that could drive basal melt of ice shelves. Recent observations have challenged both of these long-held assumptions. Geophysical observations have shown that extensive portions of the EAIS rest on bedrock below sea level (Fretwell et al., 2013). Oceanographic observations have demonstrated that relatively warm waters reach the calving fronts of glaciers that provide the major drainages of the EAIS, including the Totten Glacier (Rintoul et al., 2016; Silvano et al., 2017), the Vanderford Glacier (Herraiz-Borreguero & Naveira Garabato, 2022; Ribeiro et al., 2021), and the Denman Glacier (Brancato et al., 2020; van Wijk et al., 2022). Satellite observations confirm that several glacier systems draining the EAIS have suffered ice mass loss, grounding line retreat, and acceleration of glacial

Investigation: Natalia Ribeiro
Methodology: Natalia Ribeiro, Laura Herraiz-Borreguero, Stephen R. Rintoul, Guy Williams
Project Administration: Guy Williams, Mark Hindell
Supervision: Laura Herraiz-Borreguero, Stephen R. Rintoul, Guy Williams, Clive R. McMahon, Mark Hindell
Visualization: Natalia Ribeiro
Writing – original draft: Natalia Ribeiro
Writing – review & editing: Laura Herraiz-Borreguero, Stephen R. Rintoul, Guy Williams, Clive R. McMahon, Mark Hindell, Christophe Guinet

flow (Rignot et al., 2019; Smith et al., 2020). In both the East and West Antarctic Ice Sheet, ice loss and grounding line retreat have been linked to enhanced basal melt of ice shelves by ocean heat flux (Pritchard et al., 2012; Silvano et al., 2016).

These observations have inspired new investigations of the vulnerability of the East Antarctic ice shelves to ocean-driven melt, such as the Shackleton Ice Shelf (SIS)/Denman Glacier System (hereafter referred to as the Shackleton-Denman System; Figure 1a), an area that is now receiving close attention from the scientific community (Herraiz-Borreguero & Naveira Garabato, 2022; Urbini et al., 2010; van Wijk et al., 2022). The thinning of the SIS (Paolo et al., 2015) and retreat of the grounding line of the Denman Glacier (Brancato et al., 2020) may indicate an increase in ocean heat transport to the Shackleton-Denman System. The Shackleton-Denman System is located at the boundary of the Knox and Queen Mary Coasts of Wilkes Land, comprising three major outlet glaciers (Denman, Scott and Roscoe) and their distinctive tongues, the SIS, and an area of fast ice to the northwest of the Denman tongue (Figure 1a; Fraser et al., 2021; S. S. Thompson et al., 2023). The Shackleton polynya west of the SIS (colored contours of Figure 1b) produces 123 ± 12 Gt yr^{-1} of sea ice (Tamura et al., 2016). The Denman Glacier is on the eastern side of the SIS where there are no established polynyas and the immediate surroundings of the SIS are dominated by a fast ice region (Figure 1b; solid red line). The SIS is estimated to produce 72.6 ± 15 Gt yr^{-1} of basal meltwater, the largest among all East Antarctic ice shelves (Rignot et al., 2013). On an area-average basis, the basal melt of the SIS (2.8 ± 0.6 m yr^{-1}) is about a quarter of the area-averaged basal melt at the Totten Ice Shelf (10.5 ± 0.7 m yr^{-1}). The highest basal melt of the SIS occurs beneath the Denman Glacier, with relatively low melt rates over most of the SIS (Adusumilli et al., 2020). When compared to bigger ice shelves though, such as the Amery Ice Shelf with more than double the area of the SIS (60,654 km^2), the SIS area-average basal melt is up to 4 times higher.

Much has been learned about ocean-ice shelf interactions along the East Antarctic coast in recent years. It is now known that deep warm modified Circumpolar Deep Water (mCDW) intrusions access at least three regions of the East Antarctic continental shelf: (a) Sabrina Coast (Rintoul et al., 2016), (b) Lützow-Holm Bay (Hirano et al., 2020) and (c) Vincennes Bay (inset of Figure 1; Ribeiro et al., 2021). Most of East Antarctica's ice-mass loss occurs through Wilkes Land (100–142°E; Rignot et al., 2019). It has been suggested this ice mass loss is due to a warming of Circumpolar Deep Water (CDW) (not called modified when it is still offshore) that is linked to a southward shift of the Antarctic Circumpolar Current's southern boundary in the eastern Indian Ocean region (Herraiz-Borreguero & Naveira Garabato, 2022; Yamazaki et al., 2021), driven by a shift in the westerly winds during summer (Herraiz-Borreguero & Naveira Garabato, 2022). When warm mCDW (now modified, as it intrudes on the continental shelf) reaches the base of an ice shelf, it can drive rapid rates of basal melt.

The enhanced basal melting resulting from mCDW intrusions can freshen the waters on the continental shelf, and may hinder (Herraiz-Borreguero et al., 2016; Portela et al., 2022; Ribeiro et al., 2021) or prevent (Silvano et al., 2018) Dense Shelf Water (DSW) formation in some regions. This can generate a positive feedback, as less DSW on the continental shelf may allow more mCDW to intrude causing further melt (Herraiz-Borreguero & Naveira Garabato, 2022; Silvano et al., 2018). As DSW is the precursor of Antarctic Bottom Water (AABW), delaying or reducing DSW production may affect AABW production as well, impacting the supply of the deep limb of the global overturning circulation and, ultimately, the ventilation of the deep ocean and the global climate more generally.

As thermal forcing rises with both temperature and pressure, the rate of basal melt depends on both the temperature and the depth of the mCDW that reaches the ice shelf cavity. The Denman Glacier drains parts of the Aurora Subglacial Basin in the Wilkes Land, and holds an ice volume capable of contributing the equivalent of 1.5 m of global sea level (Rignot et al., 2019). The glacier's grounding line has retreated by more than 5 km since 1998 (Brancato et al., 2020), making it the second fastest retreating grounding line in East Antarctica. The glacier sits in the deepest marine-based basin in Antarctica (deepening to 3,400 m below sea level about 30 km from the coastline; Brancato et al., 2020), and has a steep retrograde slope (5% inclination; Brancato et al., 2020; Morlighem et al., 2020), making it potentially susceptible to irreversible retreat through marine ice sheet instability (Edwards et al., 2019). In addition, the existence of deep channels in the bathymetry over the continental shelf leading to the SIS (see dark blue arrows on Figure 1b and Supporting Information S1; Fretwell et al., 2013; McMahon et al., 2023) may facilitate the transport of mCDW to the ice cavity. Therefore, it is critical to determine the vulnerability of the Shackleton-Denman System to inflows of mCDW (van Wijk et al., 2022).

The mechanisms that transport mCDW to the Antarctic continental shelf are not well understood despite their importance for determining and quantifying the effects of changes in melt rates (Gille et al., 2016). Whether warm mCDW intrusions ($\theta > -1$°C) are a recent phenomenon or have always happened and are now more

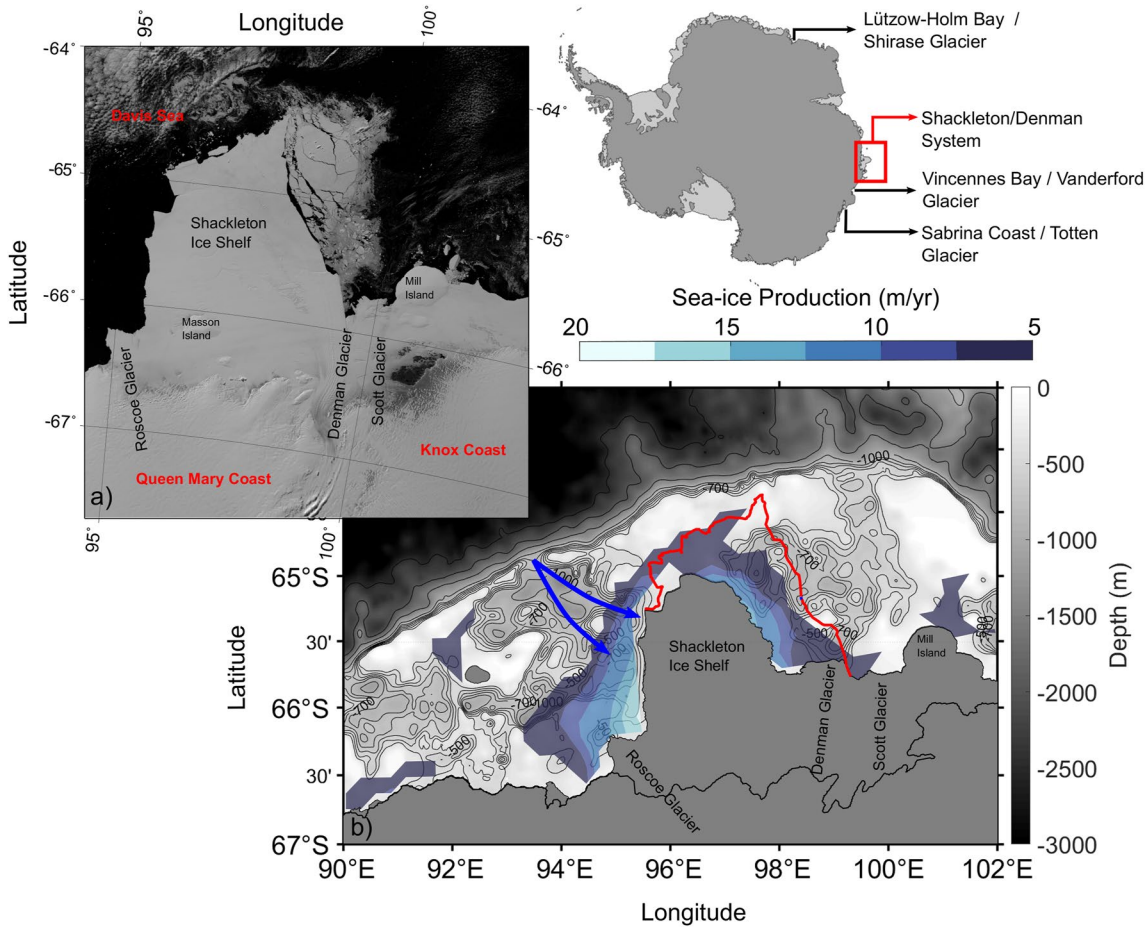

Figure 1. Study area. (a) Satellite image of the Shackleton-Denman System from 23 February 2009 (MODIS Aqua visible), with relevant geographic features highlighted in red and shelves/glaciers highlighted in black. (b) Colored contours show the 10-year (2008–2017) average sea ice production (m) around the Shackleton-Denman System (Tamura et al., 2016). Bathymetry is shown in gray shades and solid black contour lines (−400, −500, −600, −700, −800, −1,000, −1,500, −2,000, −2,500, and −3,000 m). The solid red line shows the position of the fast ice edge (digitized from Sentinel 2 surface reflectance image from 16 February 2021). The dark blue arrows indicate the position of two troughs that extend from the slope toward the ice shelf front. Bathymetry data, coastline and ice shelves are products of Bedmap2 (Fretwell et al., 2013). The inset on the top right of the figure indicates where the region sits in relation to the Antarctic continent (red box) and to relevant neighboring areas, such as Vincennes Bay (Vanderford Glacier), Sabrina Coast (Totten Glacier), and Lützow-Holm Bay (Shirase Glacier; black arrows).

obvious as a result of warming within the CDW layer (Herraiz-Borreguero & Naveira Garabato, 2022) is a topic of debate. Recent work has shown that mCDW is transported to the Totten Ice Shelf (Hirano et al., 2021) and potentially to Vincennes Bay (Yamazaki et al., 2020) by standing eddies of ≈100 km of diameter. However, the lack of data in these regions makes it difficult to determine with any certainty (a) where and how mCDW accesses the continental shelf, (b) how mCDW intrusions on the shelf vary with time, and (c) the effects of mCDW intrusions on glacial melt.

While oceanographic measurements near the SIS are relatively sparse, as in most regions around Antarctica, a set of historical profiles exists in the polynya region to the west of the SIS. In addition, a large number of oceanographic profiles have been collected in this area by instrumented elephant seals in the 2000s. The region, therefore, provides a rare opportunity to assess changes in ocean properties on the Antarctic continental shelf over a period of six decades (1956–2016). This work uses this unique data set to investigate changes in ocean properties near the SIS and is organized as follows: Section 2 describes the data in more detail, including its spatio-temporal distribution, and the methods used. Section 3 investigates changes over time in horizontal and vertical distribution of water masses, and their thermohaline properties. As changes in the amount of warm mCDW reaching the continental shelf are of particular interest, given the potential for warm ocean waters to drive rapid ice shelf basal melt (Silvano et al., 2016), Section 3.3 describes how mCDW intrusions interact with the Shackleton-Denman System. Finally, Section 4 provides a discussion of the results and Section 5 summarizes our conclusions and findings.

Table 1
Summary of Data Used From the Southern Ocean Data Base (SODB; https://zenodo.org/record/4071923#.YkKx1ChBw2w), World Ocean Atlas (WOA; Versions Prior to 2003; https://www.ncei.noaa.gov/products/world-ocean-atlas), and WOCE Global Hydrographic Climatology (WOCE; https://odv.awi.de/data/ocean/woce-global-hydrographic-climatology/)

Sample type	Country	Original database	Ship	ID	Month	Year
Bottle	Russia	woa2	OB	10299	March	1956
Bottle	Russia	woa2	OB	830	February/March	1956
Bottle	Russia	woa2	OB	4	January	1957
Bottle	Russia	woa2	OB	57	February/March	1961
Bottle	Russia	woa2	OB	9594	January/February	1964
Bottle	Russia	woa2	OB	151	January/March/April	1964
Bottle	Russia	woa2	OB	149	December	1965
Bottle	Russia	woa2	OB	9596	February/March/April	1966
Bottle	Russia	woa2	VZ	378	December	1967
Bottle	Russia	woa2	OB	282	January	1967
Bottle	Russia	woa3	OB	8396	January	1967
Bottle	Russia	woa3	OB	8401	January	1969
Bottle	Russia	woa3	VZ	411	December/January	1969
Bottle	Russia	woa2	OB	10330	January	1969
Bottle	Russia	woa2	OB	10356	January	1971
Bottle	Russia	woa2	ZB	375	January	1971
Bottle	Russia	woa3	OB	10851	January	1971
Bottle	Russia	woa3	OB	10854	January	1972
Bottle	Russia	woa2	MS	7044	April	1978
Bottle	Australia	woa2	ND	1997	January	1985
Bottle	Russia	woa3	AQ	10874	January	1988
Bottle	Russia	woa3	AQ	10876	February	1989
Bottle	Australia	woce	AR	9604_1	February	1996
CTD	Australia	woce	AR	9604_1	February	1996

Note. Country, Ship, and ID of all the data used as per the SODB.

2. Data and Methods

2.1. Data

2.1.1. Historical Oceanographic Data (1956–1996)

For this study, a total of 194 historical profiles, measured both with water sampling bottles and Conductivity-Temperature-Depth (CTD) profilers, are used. The majority are bottle profiles, but there are CTD profiles from one cruise. West of the SIS, data are available from 1956 to 1979 with two extra profiles from the 1980s and two in 1996. Data were extracted from the Southern Ocean Data Base (SODB; described in Orsi & Whitworth, 2005, ; https://zenodo.org/record/4071923#.YkKx1ChBw2w), World Ocean Atlas (WOA; versions prior to 2003; https://www.ncei.noaa.gov/products/world-ocean-atlas), and WOCE Global Hydrographic Climatology (WOCE; https://odv.awi.de/data/ocean/woce-global-hydrographic-climatology/). Details of the data used here are provided in Table 1.

To focus on the continental shelf, only data that were located at least 0.3° of latitude south of the 1,000 m isobath (commonly used to separate the coast from the offshore waters) were included. This threshold was chosen to exclude profiles that had high bottom temperatures (≈0°C; not shown) near the slope, as it was likely they were sampling over the slope rather than on the continental shelf. Primary interest was in full-depth profiles

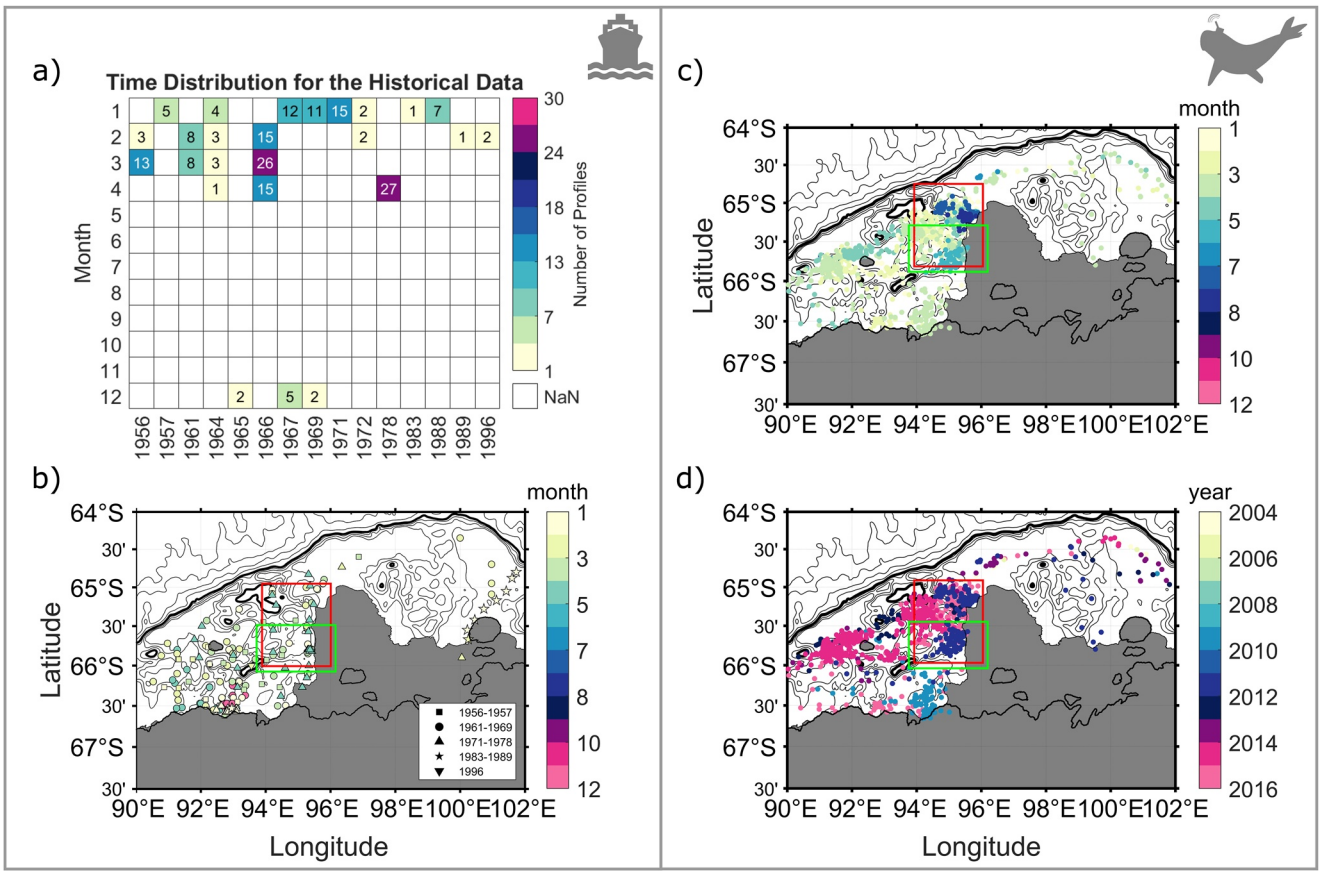

Figure 2. Spatio-temporal distribution of data. (a) Heatmap with number of profiles per month and year for the historical data. (b) Time distribution in relation to space for the historical data. (c) Monthly and (d) yearly distribution in relation to space for the biologging data set. Boxes show the regions where modified Circumpolar Deep Water (red) and Dense Shelf Water (green) property changes are analyzed in detail (Section 3.2). The −400, −600, −800, −1,500, −2,000, and −3,000 m bathymetric contours are shown in black thin lines and the −1,000 m contour is highlighted by the thick black line. Hereafter, the boat symbol is added to the subplots that have historical data, while the seal symbol is for data retrieved by instrumented elephant seals.

but determining which profiles have reached the bottom can be challenging given the uncertainty in available bathymetry (median error in the bathymetry ranging from ≈100 to 260 m within 20 km from ship track data; Fretwell et al., 2013). Most of the historical data included metadata indicating the bottom depth (171 profiles). For those that did not have this information available, manual checks were done and profiles were only kept if (a) they reach the bottom (or deeper), (b) they do not reach bottom but are deeper than the thermocline or (c) they are within 100 m of the bottom, but the vertical structure is consistent with a full-depth profile. The data only cover summer and autumn (December to April), with the highest number of profiles returned between March and April (Table 1; Figures 2a and 2b). The data were not interpolated to standard depths, although a few profiles extracted from the data base appear to have been interpolated before being added to the compilation.

The CTD data offer an accuracy of 0.001°C for temperature and 0.005 for salinity (Gouretski & Reseghetti, 2010; Thomson & Emery, 2014). Bottle data were generally equipped with reversing thermometers that, when protected and well calibrated, are accurate up to 0.01°C or better (Abraham et al., 2012). Generally, bottle salinity was measured by ship-based salinometers, and inductive systems from the 1960s had an accuracy of approximately 0.003 ppm (Brown & Hamon, 1961).

2.1.2. Biologging Data (2004–2016)

The Antarctic continental shelf remains one of the least sampled regions on Earth (McMahon et al., 2021) due to the inherent logistic challenges relating to sea ice and weather (Harcourt et al., 2019; Roquet et al., 2014; Treasure et al., 2017; G. D. Williams et al., 2016). Seal CTD-SRDL (Conductivity-Temperature-Depth Satellite Relay Data Logger) data (MEOP consortium—Marine Mammals Exploring the Oceans Pole to Pole; www.meop.net)

Table 2
Elephant Seal Data Identification (90–102°E)

Seal tag	No. of profiles in study area	Start date	End date
00008	11	24/3/2004	24/3/2004
10029	2	27/3/2004	15/4/2004
00013	11	27/3/2005	31/3/2005
00184	1	3/3/2009	31/3/2009
00019	28	20/2/2009	20/2/2009
00024	9	23/8/2009	07/9/2009
00254	38	21/2/2011	19/8/2011
00046	8	9/9/2012	09/9/2012
00047	171	5/4/2012	16/4/2012
00049	299	26/2/2012	28/2/2012
00744	7	4/4/2012	26/4/2012
00875	42	9/3/2013	15/3/2013
09118	1	5/3/2013	14/3/2013
00942	9	10/3/2013	13/3/2013
00949	38	19/03/2014	2/4/2014
00968	244	21/1/2014	21/3/2014
09929	15	25/01/2014	26/4/2014
"A"	97	24/1/2015	30/1/2015
"Cy24"	265	17/02/2015	3/3/2015
"E"	1	14/01/2015	15/4/2015
"F"	3	31/3/2016	3/4/2016

Note. Data retrieved from the MEOP consortium (Marine Mammals Exploring the Oceans Pole to Pole; www.meop.net).

have been addressing this critical data gap since 2004 and now constitute the bulk of the oceanographic profiles available near the Antarctic margin. For this study, a total of 1,300 CTD-SRDL profiles in the Shackleton-Denman System are available from 21 seal-borne tags across various deployment locations (Table 2). Only profiles that are 0.3° of latitude south of the 1,000 m isobath were included, to ensure all profiles used were on the continental shelf. The data cover most of the year from January to November, with the highest number of profiles returned between February and May (Table 2; Figures 2c and 2d).

The CTD-SRDL records the ascending profiles at 1 Hz, retaining only the deepest dive within a six-hour period. The location of the individual profiles is provided by the Advanced Research and Global Observation Satellite (ARGOS) system, precise to within a few kilometers using the data processing method described in Roquet et al. (2017). While CTD-SRDL data are less accurate than ship-based measurements (bottles and CTD), there has been ongoing development of the post-processing protocols (Jonsen et al., 2020; Mensah et al., 2018; Siegelman et al., 2019). The final accuracy of the salinity and temperature data is estimated to be ±0.03 and ± 0.04°C, respectively (Siegelman et al., 2019).

2.1.3. Spatio-Temporal Distribution of Available Historical and Seal Data

The time distribution (months and years) of the profiles is shown in relation to space (Figure 2). The historical data cover the area until the end of the 1970s, which is then followed by a big gap through the 1980s and 1990s. The biologging data begin in the 2000s and become the main source of data.

The heatmap in Figure 2a shows that there are no historical data available for the winter months and that most of the profiles were obtained before the 1980s, more precisely between the 1960s and 1970s. Most of the historical profiles were collected during summer (n = 100) and at the beginning of autumn (n = 93), with one profile from late spring (Figures 2a, 2b, and 3). The east of the SIS has fewer measurements, mostly on the outer shelf and obtained in the 60 and 80s (Figures 2b and 3).

The biologging data set is more numerous (194 historical compared to 1,300 seal CTD-SRDL profiles) and, although more profiles correspond to summer (412 profiles) and autumn (795 profiles) months, it contains some unique profiles over winter (93; Figures 2c and 3). The biologging data set spans the period from 2004 to 2016, with the most densely sampled years being 2011, 2014, and 2015 (Figures 2d and 3). The red and green boxes (Figures 2b–2d and 3) highlight regions with reasonable coverage in the same season across both the historical and biologging data sets. These regions are explicitly used to discuss longer-term changes in mCDW and DSW in Section 3.2.

2.2. Water Mass Definitions and Time Distribution

Here, we introduce the key water masses and their temporal distribution across the available data. The cold and fresh surface layer south of the Polar Front, known as Antarctic Surface Water (AASW), is formed in winter through convection driven by atmospheric cooling and brine rejected during sea ice growth. In the summer, a warmer sub-layer (≈50 m) forms at the surface from the melting of sea ice, overlying a cold subsurface layer from the previous winter. This temperature minimum layer within the AASW is referred to as Winter Water (WW; Whitworth et al., 1998). Warmer and more saline CDW lies below the AASW and is isolated from atmospheric cooling. Where intrusions of CDW do reach the continental shelf, the water properties are altered by mixing to form a cooler water mass known as modified CDW (mCDW). Conventionally, waters that are less dense than CDW are classified as AASW (Whitworth et al., 1998), thus we use neutral density layers to separate the two water masses (Table 3).

Table 3
Classification of the Water Masses in the Shackleton-Denman System

Water mass	γ^n (kg m^{-3})	θ (°C)	Practical salinity
AASW	$\gamma^n < 28$		
WW	$27.55 < \gamma^n < 28$	$\theta < -1.8$	
mCDW	$28 < \gamma^n < 28.27$	$-1.7 < \theta < 1.5$	
DSW	$\gamma^n > 28.27$	$-1.92 < \theta < -1.8$	$S > 34.4$
ISW		$\theta < -1.92$	

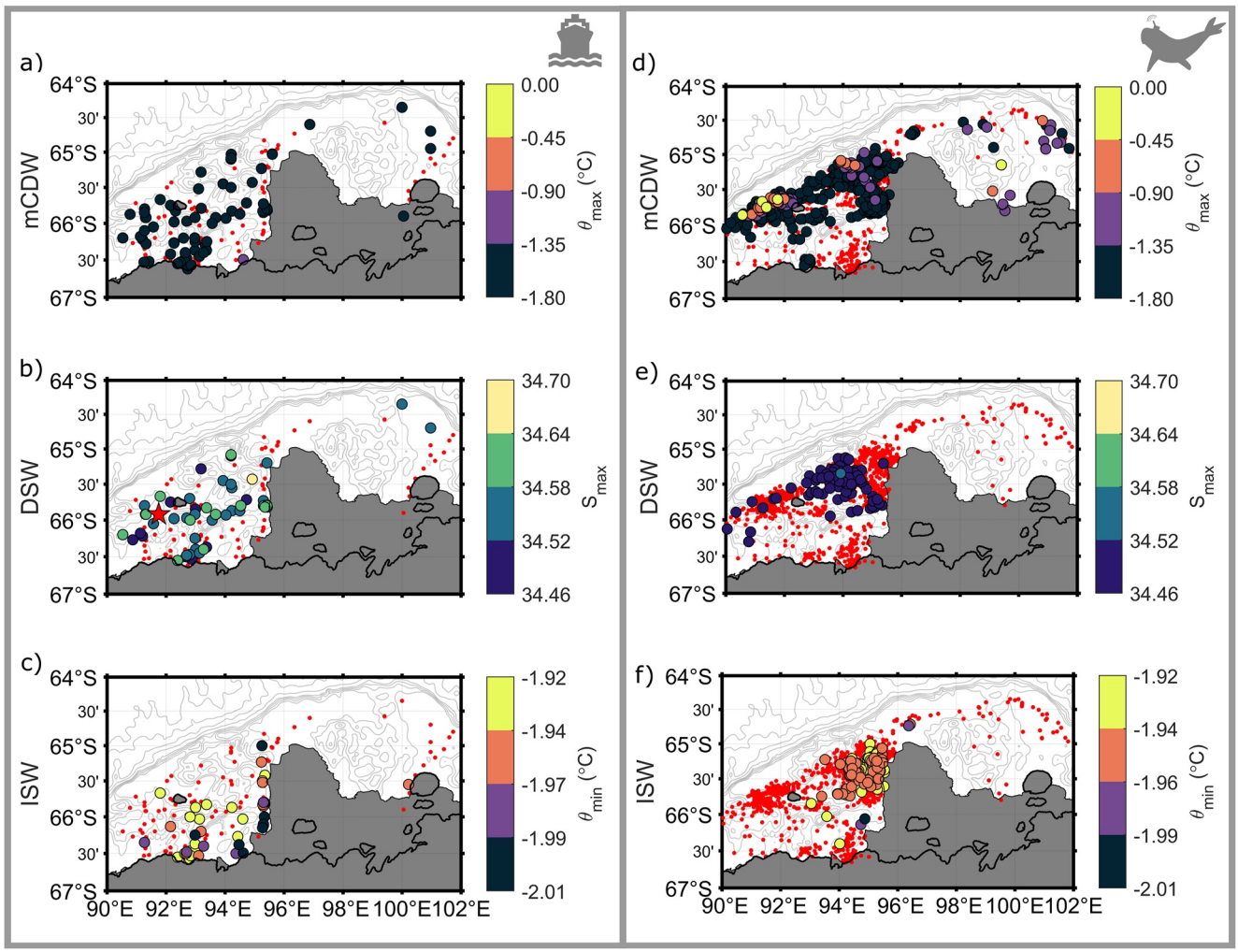

Figure 3. Thermohaline properties for modified Circumpolar Deep Water (mCDW), Dense Shelf Water (DSW) and Ice Shelf Water (ISW). (a) Maximum mCDW potential temperature (°C), (b) maximum DSW salinity, and (c) minimum ISW potential temperature (°C) for the historical data; (d) maximum mCDW potential temperature (°C), (e) maximum DSW salinity, and (f) minimum ISW potential temperature (°C) for the biologging data set. The red star in (b) shows the position of the maximum salinity value of 34.8 that was kept out of the color scale to allow comparison with the seal data. The red dots represent the remaining profiles from each data set that do not contain the specific water masses depicted in each plot. The −400, −600, −800, −1,000, −1,500, −2,000, and −3,000 m bathymetric contours are shown by the solid gray lines. Historical data (boat symbol) comprise data between the years of 1956–1996 and the seal data (seal symbol) comprise data retrieved between the years of 2004–2016. Bathymetry data, coastline and ice shelf contour are from Bedmap2 (Fretwell et al., 2013).

DSW is formed through winter convection in areas of strong sea ice formation, such as coastal polynyas. Where DSW is present, it is the densest water on the shelf and can access deep ice shelf grounding lines (Nicholls et al., 2009) in what A. F. Thompson et al. (2018) described as a "dense shelf." Accordingly, where DSW is absent and mCDW is present, the coastal ocean regime is characterized as "warm shelf" (A. F. Thompson et al., 2018). When mCDW is the densest water on the shelf, occupying the bottom layer (as e.g., seen near the Totten Ice Shelf and in Vincennes Bay; Ribeiro et al., 2021; Silvano et al., 2017), much warmer water can reach the deep ice shelf grounding lines. Where neither DSW nor mCDW are present, AASW will occupy the full water column, corresponding to a "fresh shelf" classification (A. F. Thompson et al., 2018).

All shelf water masses (AASW, WW, mCDW, DSW) can potentially drive the melting of ice shelves given the pressure dependence of the freezing point of sea water (Foldvik & Kvinge, 1974). Warm water reaching the ice shelf at depth will have the strongest thermal forcing and the characteristics of the meltwater mixture leaving the cavity will depend on the properties of the water driving the melt. In cold-cavity ice shelves where DSW drives melt near the grounding line, the mixture formed by mixing of meltwater with DSW may exit the cavity with a temperature below the surface freezing point, known as Ice Shelf Water (ISW). In warm-cavity ice shelves, where

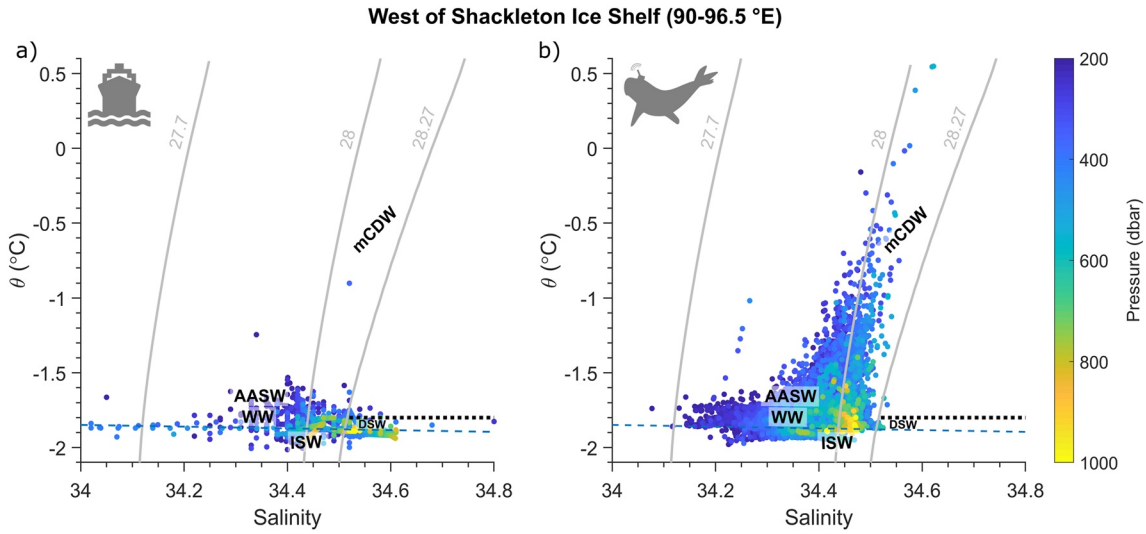

Figure 4. Potential temperature (°C)/salinity relationship (a) for the historical and (b) for the biologging data set within the west of the Shackleton Ice Shelf domain (90–96°E). Data points are color-coded by pressure (dbar). The γ^n isopycnals of 27.7 (Winter Water; WW), 28 (modified Circumpolar Deep Water; mCDW) and 28.27 kg m^{-3} (Dense Shelf Water; DSW) are shown in gray in both panels. The horizontal black dotted line indicates the upper limit of DSW's temperature definition ($\theta = 1.8$°C). Seawater surface freezing point, which is also the lower limit of DSW's temperature definition to the right of the 28.27 kg m^{-3} isopycnal, is shown by the horizontal light blue dashed line.

mCDW drives melt near the grounding line, the meltwater mixture may have a temperature higher than the surface freezing point and therefore not be classified as ISW. To classify the water masses in the Shackleton-Denman System, we use the same classification used in Ribeiro et al. (2021) for Vincennes Bay, which is immediately upstream. Water mass properties are described in Table 3.

3. Results

3.1. Horizontal and Vertical Distribution of Water Masses

In the next two subsections we investigate the distribution of water masses on the continental shelf surrounding the Shackleton-Denman System, assessing the historical data (Figures 3a–3c) and the biologging data set (Figure 3d–3f) independently.

3.1.1. Historical Data

Figure 3 shows the spatial distribution of mCDW, DSW, and ISW across the region. West of the SIS (90–96.5°E), only a very cold variety of mCDW ($-1.75 < \theta < -1.6$°C) can be seen over the shelf in the historical data. The average maximum potential temperature for this mCDW was -1.7 ± 0.12°C (uncertainties associated with the data sets utilized in this study represent one standard deviation unless otherwise specified). Cold mCDW occupies most of the continental shelf at depths shallower than 400 dbar (Figure 4a), except in the nook formed by the southern end of the shelf and the Antarctic margin (≈94–96°E) where a single profile (66.5°S/94.7°E) shows mCDW with a temperature of −0.9°C at ≈350 dbar. East of the SIS (97–102°E), mCDW is not present near the ice front, with the exception of one profile that shows cold mCDW at the edge of the Scott Glacier. Given the calving front of the Scott Glacier advanced about 10 km from 1962 to 1991 before retreating back to the same position it was in 1962 in recent years (S. S. Thompson et al., 2023), this profile was likely to be near the ice front rather than underneath it, as Figures 2 and 3 might suggest. Data from the east of the SIS are limited though, and mostly sampled in shallower areas, meaning the possibility of a wider presence of mCDW, especially at depth, should not be discarded.

The spatial distribution of DSW (Figure 3b) is similar to the mCDW. DSW is found west of the SIS, with an average salinity maximum of 34.54 ± 0.05. Out of 68 profiles that recorded DSW, about 30% registered salinity maxima over 34.6, with the two highest values being 34.68 and 34.8 (red star, Figure 3b). No DSW is recorded to the east of the SIS except for two profiles close to the slope. The fact that the eastern side has a significant portion of fast ice and no consistent polynya regions, makes it unlikely that a significant amount of DSW would be formed there. Yet, because of the lack of data in the area, DSW presence on the eastern

side of the SIS can't be ruled out. ISW (Figure 3c) is found along the western edge of the SIS and along the coastal margin, with the coldest varieties ($\theta < -1.95$°C) mostly limited to the small nook where the ice shelf extends from the coast as the Roscoe Glacier. Slightly warmer ISW is recorded in the center of the basin, with temperatures ranging from −1.92 to −1.94°C. In the east, one profile records ISW ($\theta = -1.96$°C) on the edge of Scott Glacier.

Overall, the historical data paint the picture of a cold continental shelf (A. F. Thompson et al., 2018) west of the SIS: (a) no warm intrusions of mCDW ($\theta \geq -1$°C) from offshore, with only cool varieties being found over the shelf and at depths shallower than 500 dbar (see Figure 4a); (b) a local polynya that produces DSW with high salinity ($S \geq 34.54 \pm 0.05$); and (c) DSW occupying the bottom layer as the densest water on the shelf (see Figure 4a).

3.1.2. Biologging Data

In contrast to the historical data, the more recent biologging data set (2004–2016) shows a very different distribution of water masses (Figures 3d–3f). Specifically, the seal data show that mCDW is now the dominant water mass on the western continental shelf (Figure 3d). The maximum temperature on most profiles remains below −1.35°C, however an early autumn (March-April; Figure 2c) mCDW intrusion in 2011 (Figure 2d), with a maximum temperature of −0.6°C, approaches the western side of the SIS and cools to −1.2°C when it reaches the ice shelf front (Figure 3d). Warmer mCDW ($-1.35 < \theta < -0.45$°C) is found where deeper topography extends from the shelf break to the SIS. This suggests that the mCDW pathway toward the SIS is along this deeper topography, splitting into two deep troughs near the ice shelf (see dark blue arrows in Figure 1b). In the historical profiles, mCDW temperatures were always below −1.6°C in the same region (Figure 3a) and at the same period of the year (Figure 2b; see Text S1 and S2 in Supporting Information S1 for details on mCDW pathway). The nook formed by the western edge of the SIS and the coast, where the Roscoe Glacier is situated, is sampled by the seals (gray transparent dots), but no mCDW is recorded there.

In addition to the seal profiles collected west of the SIS, a few profiles were gathered to the east (data also shown in Brancato et al., 2020). In March 2011 (Figures 2c and 2d), a rift in the fast ice allowed one seal to reach the eastern side of the Shackleton-Denman System. The warmest mCDW seen in the whole data set was recorded in these profiles, with a maximum temperature of −0.29°C at a depth of 852 dbar and with 127 m of thickness (65.1°S; 99.4°E), and water as warm as −0.7°C near the edge of the Denman Glacier at 782 dbar and with 57 m of thickness (65.5°S; 99.1°E). Profiling float observations on the continental shelf near the Denman Glacier, east of the SIS, also show mCDW as warm as −0.16°C reaching a deep trough extending beneath the Denman Ice Tongue (van Wijk et al., 2022). The ocean heat transport estimated from the float observations is sufficient to drive high rates of basal melt of the Denman Glacier that are consistent with those estimated from satellite data (van Wijk et al., 2022). However, the pathway of the mCDW from the shelf break to the ice front remains unknown. Moreover, given the lack of in situ historical measurements, it is not possible to determine if the distribution, volume or temperature of mCDW on the eastern shelf has changed over time.

In the seal data, the distribution of DSW (Figure 3e) is confined to the west of the SIS and away from the coast (north of 66°S, 94–95°E) in the channel where bathymetry is deeper than 700 m. The salinity maximum is much lower than seen in the historical data, with the seals showing an average salinity maximum for DSW of 34.48 ± 0.01, compared to the 34.54 ± 0.05 from the historical data set. Of 129 seal profiles with DSW present, 85% recorded maximum salinity values under 34.5, against only 11% of the 70 historical profiles with DSW.

About 85% of the 106 seal profiles with ISW present temperatures above −1.95°C, which is warm in comparison to the historical data set, where only 53% of the 46 profiles feature temperatures above this threshold. Cold ISW (≤ -1.95°C) is found in only 15% of the seal profiles and, although the seals foraged south of 66°S, only three profiles found ISW there (Figure 3f). Similar to DSW, the observed ISW is mostly clustered north of 65.5°S and near the SIS (94.5–96°E).

The initial results show that the properties and distribution of each of the water masses vary over time, with the most noticeable changes in the absence (historical data set)/presence (biologging data set) of mCDW and in the salinity of DSW that decreases significantly from one data set to the other. Overall, the comparison of the recent seal data to the historical data indicates that the region west of the SIS seems to have transitioned over the past 60 years from a classical “cold” Antarctic Ice Shelf to a relatively warmer shelf, with a different distribution of water masses.

3.1.3. Potential Temperature-Salinity (θ-S) Distribution of Water Masses for Historical and Biologging Data

The distribution of water masses west of the SIS for historical (a) and seal (b) data is shown in Figure 4, using θ/S curves color-coded by pressure. Before 1996, mCDW and DSW occupy similar areas of the continental shelf, but the denser DSW is found below the mCDW. mCDW is present between 400 and 500 dbar and DSW is present below 500 dbar (Figure 4a). Ice Shelf Water (ISW) occupies a range of depths (200–700 dbar), but is most commonly found between 200 and 400 dbar. The salinity range of ISW is wide, spanning from 34 to 34.6.

The θ-S curves for the seal data show large differences west of the SIS compared to the historical data (Figures 4a and 4b). Colder varieties of mCDW are observed as deep as 1,000 dbar (-1.7 to -1.5°C), while warmer intrusions are consistently found between 200 and 600 dbar ($\theta > -1$°C). Dense Shelf Water (DSW) is no longer the only water mass occupying the deeper layers over the continental shelf, and, at times, it may not be present. There are very few data points of DSW ($\gamma > 28.27$ kg m^{-3}) and they are all from the month of April. The salinity range for ISW still varies widely (≈34.2–34.4), and this is reflected on the vertical distribution of ISW which ranges from 200 dbar down to 700 dbar (Figure 4b and inset of Figure 5c). Additionally, it is worth noting there is no ISW denser than $\gamma > 28.27$ kg m^{-3}.

While the differences in water mass properties and presence are significant, changes in their vertical distribution are of particular importance for ocean-ice shelf interactions. In the historical data, DSW was saltier and denser than the DSW recorded in the seal data set, and dominated the bottom layer over the deepest part of the continental shelf. It sits on average below 491 m with an average thickness of 313 m (estimates calculated within the mCDW box domain; red box in Figures 2b–2d). The biologging data set shows that this has changed, with the DSW thickness reduced to 60 m and DSW no longer occupying a significant part of the continental waters, instead being confined to depths below 710 dbar on average when present. Now, mCDW is found at depths previously occupied by DSW (average minimum depth of 395 dbar and 146 m of average thickness) and its average thickness has more than tripled (40 m in the historical data set). This has implications for ice shelf stability, as warm mCDW at depth has the potential to access the ice shelf cavity (bathymetry allowing), where it can drive stronger basal melt than observed when the significantly colder DSW reaches the cavity.

3.2. Interannual to Decadal Variability

An overview of the temporal changes occurring to the west of the SIS is shown in Figure 5, where the vertical distribution of both data sets are plotted together. Differences in salinity and temperature can be seen at all depths. The more recent seal profiles are fresher throughout the water column, by up to 0.02 at 400 dbar and about 0.1 in the other layers (Figure 5b). While the historical data did not record any temperatures above -1.6°C below 200 dbar, the biologging data set shows a recurrent presence of mCDW at mid-depths between 200 and 600 dbar (Figure 5c). Maximum temperature recorded values at 600 dbar are 1.2°C higher in the biologging data set, reaching a maximum value of -0.4°C, and temperatures are consistently higher across all depths when compared to the historical data. Both the averaged salinity (Figure 5d) and potential temperature (Figure 5e) per pressure show that the changes in properties between the data sets are significant.

The temporal evolution of water mass properties and bottom potential temperature (purple) and salinity (orange) for the continental shelf west of the SIS is shown in Figures 6a–6d. The temporal evolution is shown as an average of the profiles available in each year or the actual value when limited to a single profile. For the ISW maximum temperature (Figure 6b), the west of the SIS domain (90–96°E) is used. To avoid aliasing of spatial or seasonal variability, we compare the bottom potential temperature and salinity (θ/S; Figure 6a), and the average maximum potential temperature and salinity for mCDW (Figure 6c) constraining the analysis to the profiles within the red box at 65–66°S/94–96°E (mCDW domain; Figures 2b–2d). For DSW (Figure 6d), we use the profiles within the green box at 65.5–66°S/94–96°E (DSW domain; Figures 2b–2d). Only historical profiles that reached the bottom are included in the bottom θ/S time series (Figure 6a).

In general, the seal profiles (squares) available for this analysis are more numerous (>30; see bars in Figures 6a–6d). Both data sets sample DSW (Figures 2b–2d, green box; Figures 3d–3f) along the same months of the year (January to April). For mCDW, the area is larger and some winter profiles in the north are included in the biologging data set. They make up only 14% of the profiles in the box, and excluding them does not change the time series trends (not shown). In the historical data (circles), all profiles are from summer or early autumn, which is when mCDW is found near the edge of the SIS in the seal data (Figure 2c) and the strongest mCDW intrusions are recorded in nearby Vincennes Bay (Ribeiro et al., 2021).

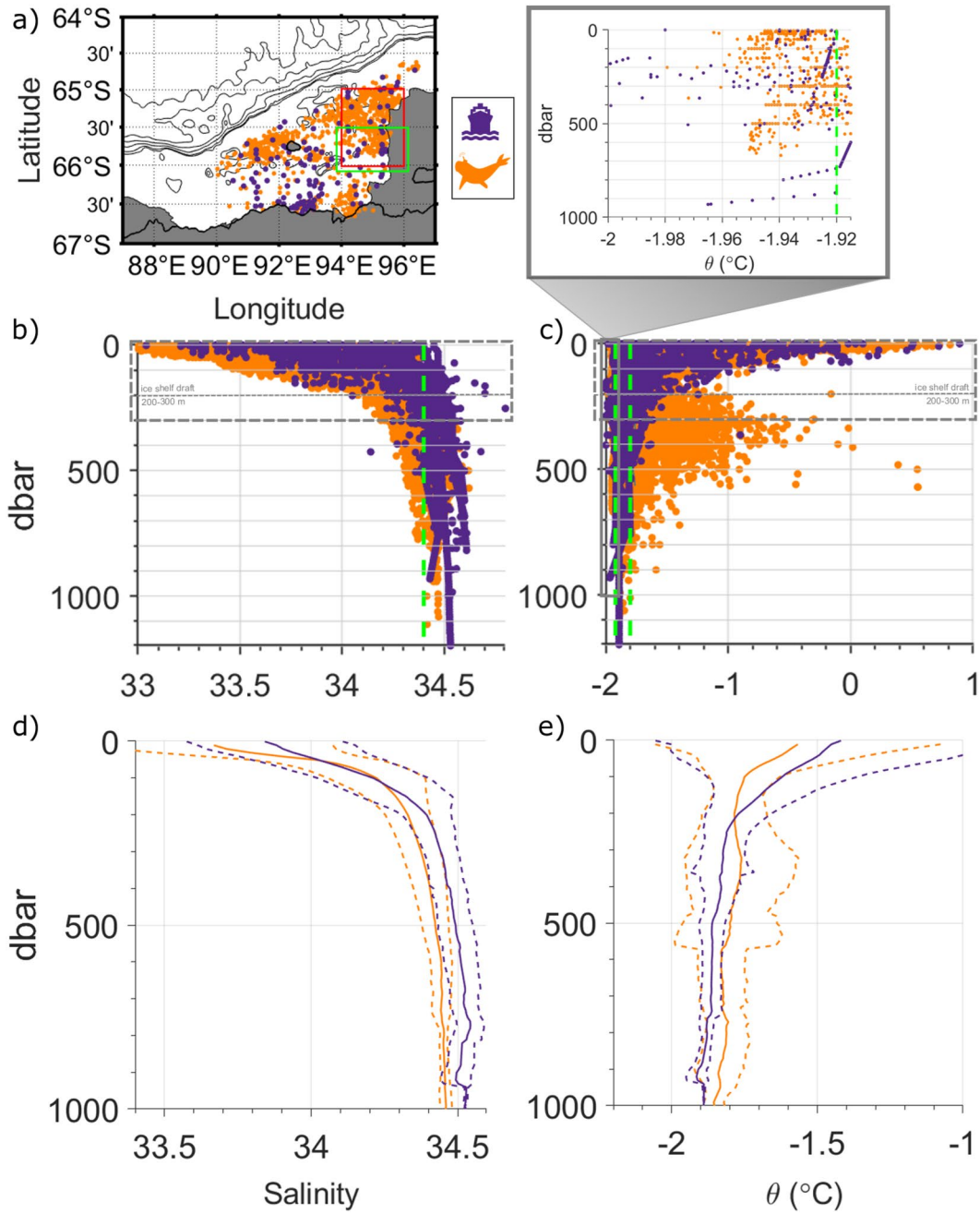

Figure 5. Full data set comparison on the western side of the Shackleton Ice Shelf. (a) The map shows the spatial distribution of the data. The boxes show the region where modified Circumpolar Deep Water (mCDW; red) and Dense Shelf Water (DSW; green) properties' changes are analyzed in detail in Section 3.2. Data are then displayed in vertical profiles of (b) salinity and (c) potential temperature (°C), with panels (d) and (e) showing the same salinity and potential temperature data as pressure-averaged profiles (solid line) with one standard deviation (dashed line). A separated inset in (c) zooms in on the ISW's ($\theta < -1.92$°C) distribution. Historical data (1956–1996) are shown in purple and seal data (2004–2016) are shown in orange. Dashed vertical green lines indicate the lower salinity limit for DSW (34.4) in (b) and in the inset, and the higher temperature limit for Ice Shelf Water (ISW; −1.92°C) and DSW (−1.8°C) in (c). The ice shelf draft (200–300 m; Urbini et al., 2010) is indicated by the vertical double gray-dashed rectangle.

Before the 1980s, DSW is consistently found west of the SIS, with temperatures below −1.8°C (Figure 6a). From 2009, bottom temperatures exceed −1.6°C and particularly warm values are observed in the two well-sampled years of 2011 and 2014. The bottom salinity is lower by about 0.09 on average after 2009, when compared to the mean values prior to 1980. Temperature changes can be seen in ISW as well (Figure 6b), but they are not significant.

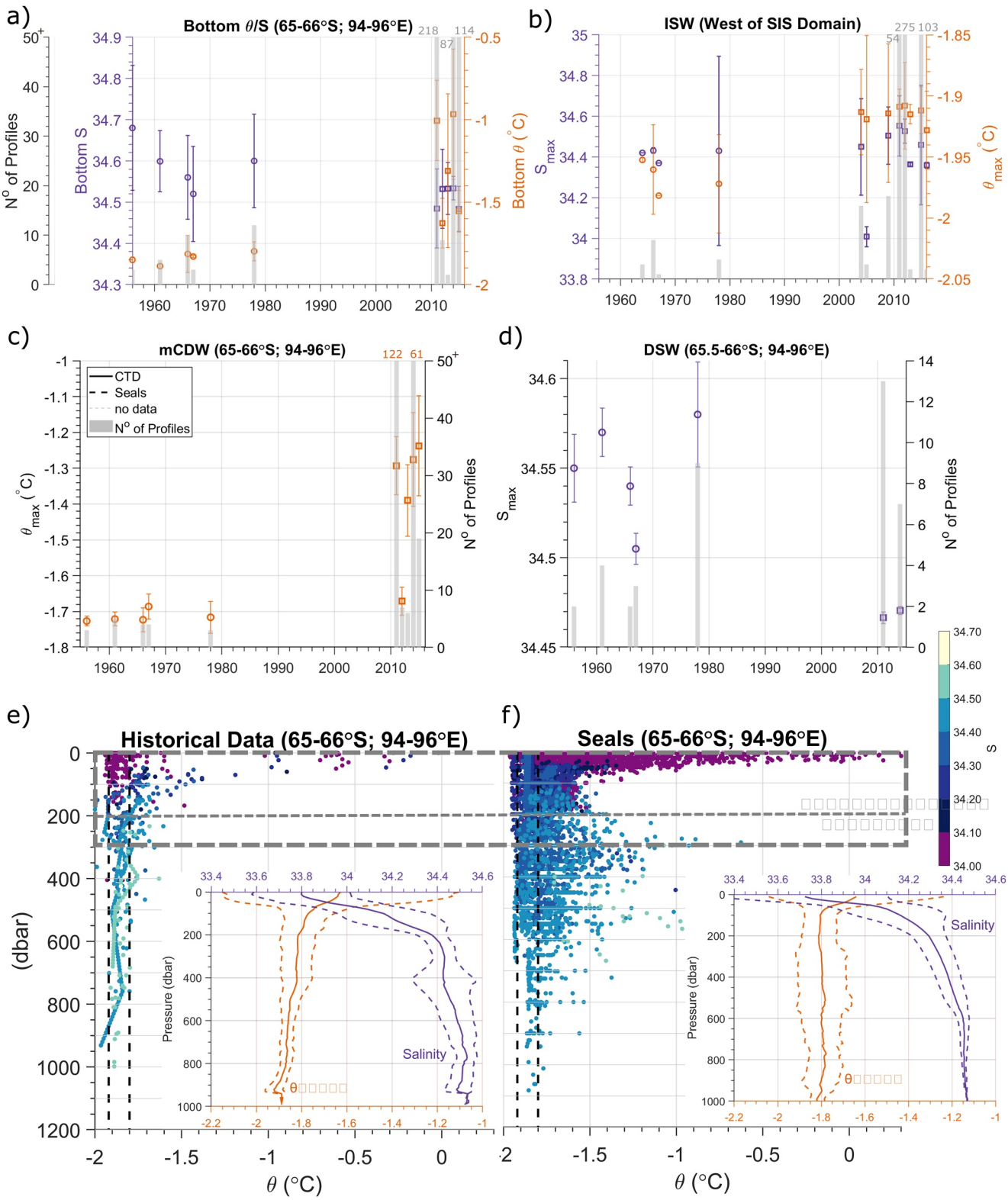
a)
Bottom θ/S (65-66°S; 94-96°E)
N° of Profiles
Bottom S
Bottom θ (°C)
b)
ISW (West of SIS Domain)
S max
θ max (°C)
c)
mCDW (65-66°S; 94-96°E)
CTD
Seals
no data
N° of Profiles
θ max (°C)
d)
DSW (65.5-66°S; 94-96°E)
S max
e)
Historical Data (65-66°S; 94-96°E)
f)
Seals (65-66°S; 94-96°E)
(dbar)
θ (°C)
Pressure (dbar)
Salinity
θ
S

Figure 6.

The maximum temperature for mCDW captures two particularly warm events in 2011 and 2014, but also shows warm intrusions in the other two years (Figure 6c). In 2013 and 2015, the maximum temperature reached −1.2°C close to the western edge of the SIS calving front. By comparison, in the historical data set the maximum temperature of mCDW in the same area didn't exceed −1.6°C. DSW also shows pronounced changes, with its average maximum salinity dropping by 0.08 (Figure 6d), when comparing data before and after 1980. The average salinity of DSW is 0.07 higher in the historical data.

When looking at the vertical θ/S profiles within the mCDW box (which includes the DSW box; Figures 6e and 6f), we can see how the data sets compare at depth. mCDW intrusions were not present in the area before 1980 (Figure 6e; inset shows averaged profiles for temperature and salinity). From 1980 to 2008 there is a gap in the data available. After 2009, mCDW intrusions are observed at many profiles, primarily at mid-depths (200–600 dbar) and occasionally at deeper depths (Figure 6f; inset shows averaged profiles for temperature and salinity). Dense Shelf Water (DSW; colored dots in-between the two vertical dashed lines in Figures 6e and 6f) is fresher in the seal data (Figure 6f) at all observed depths than in the historical data (Figure 6e). The wide salinity range for ISW is once again reflected in both data sets, but in the seal data, temperatures are closer to the upper limit of the ISW temperature definition.

Overall the results demonstrate the modern seal profiles are fresher and warmer than the historical profiles (Figures 3, 5 and 6). Comparison of profiles in the mCDW domain box shows that warm mCDW intrusions did not occur before 1980, but occurred every year from 2011 (Figures 3 and 6c). At the same time, DSW maximum salinity is 0.08 fresher in the biologging data set (34.47) than it was in the historical data set (34.55). In Section 3.3, we investigate how warm mCDW interacts with the Shackleton Ice Shelf to determine if the observed changes in mCDW and DSW properties are a reflection of ocean-driven basal melt.

3.3. mCDW Intrusions Underneath the Shackleton Ice Shelf

Potential temperature-Salinity (θ-S) curves illustrate the changes in the properties and distribution of the key water masses (mCDW, DSW, ISW) over time (Figure 7). West of the SIS, DSW is present in the historical data, occupying a wide range of salinity values, but with salinity consistently greater than 34.5 (Figure 7a). In contrast, DSW is noticeably reduced in the seal data (Figures 7b–7d). The two data sets cover both summer (January-February, with a few profiles in Dec from the historical data) and autumn (March-April, with a few profiles in May from the seal data), so the difference between them cannot be explained by seasonal aliasing. The differences are even more striking when considering the temperature of mCDW. Before 1996, mCDW with temperatures greater than −1.6°C (Figure 7a) is rarely observed, constituting only 2.6% of all mCDW recorded in the historical data set. After 2004, 44.3% of the mCDW recorded on the continental shelf west of the SIS had temperatures above −1.6°C, with about 30% being warmer than −1°C, and some values even exceeding 0°C (Figure 4b).

We use the Gade Line (Gade, 1979), a useful tool to understand meltwater mixtures, to show how DSW and mCDW interact with the SIS. The Gade equation assumes that sensible heat transfer from the ocean to ice is negligible compared to the energy used for ice melting (latent heat) and that the volume of meltwater is small compared to the volume of the ocean (Gade, 1979; Jenkins, 1999). The equation draws a line in the θ/S space, linking meltwater with the source water mass producing it, in the absence of mixing with other water masses. This line is known as the melt-freeze line and it is defined by,

Figure 6. Time series of water mass properties between 1956 and 2016 on the west of the Shackleton Ice Shelf (SIS). (a) Time series of bottom salinity and its respective potential temperature (°C) inside the defined modified Circumpolar Deep Water (mCDW) domain (red box in Figures 2b–2d; 65–66°S; 94–96°E). (b). Time series of maximum salinity and maximum potential temperature (°C) of Ice Shelf Water (ISW) present in the whole area comprising the west of the SIS (90–96.5°E). (c) Time series of maximum potential temperature (°C) of mCDW inside the defined mCDW domain (red box in Figures 2b–2d; 65–66°S; 94–96°E). (d) Time series of maximum salinity of Dense Shelf Water (DSW) inside the defined DSW domain (green box in Figures 2b–2d; 65.5–66°S; 94–96°E). Circles represent the historical data and squares the seal data. Error bars represent two standard deviations within each year average and histogram bars show the number of profiles used in each average. Salinity and potential temperature time series are showed in orange and purple, respectively. (e) The historical and (f) the biologging data sets within the mCDW domain (red box in Figures 2b–2d; 65–66°S; 94–96°E) are also displayed in vertical potential temperature profiles (°C), with data points color-coded by their respective salinity values. Dashed vertical black lines indicate the higher temperature limit for ISW (−1.92°C) and DSW (−1.8°C) in (e) and (f). Pressure-averaged profiles (solid line) with standard deviation (dashed lines) of temperature (orange) and salinity (purple) are provided for each data set as insets in (e) and (f). The ice shelf draft (200–300 m; Urbini et al., 2010) is indicated by the double gray-dashed rectangle.

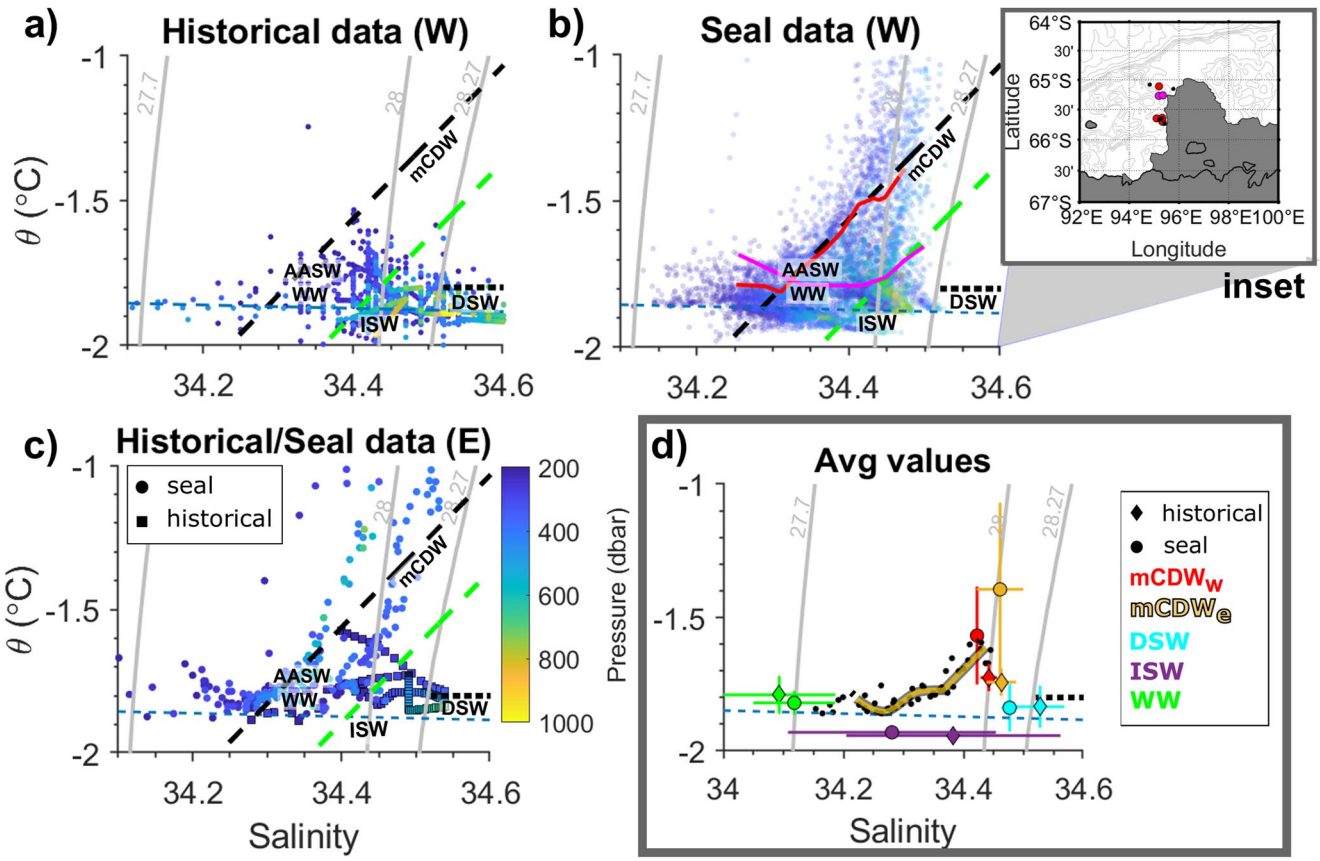

Figure 7. Temporal evolution of the water masses for the Shackleton-Denman System. (a) Historical (1956–1996) and (b) seal data (2004–2016) west of the Shackleton Ice Shelf (SIS) are displayed in the θ-S space, color-coded by pressure (dbar). Seal profiles that fit the Gade lines are averaged and displayed in red (black dashed line; $\theta = -1.4$°C, $S = 34.46$) and pink (green dashed line; $\theta = -1.55$°C, $S = 34.46$). A map inset shows the position of these profiles in relation to the SIS. (c) Water mass distribution for the east of the SIS with both historical data (square) and seal data points (dots) color-coded by pressure (dbar). (d) A θ-S diagram, illustrating average values for different water masses within the west and east regions of the SIS is highlighted by a gray rectangle. Specifically, Winter Water (WW) (green; representing the average of the west of the SIS domain), Ice Shelf Water (ISW) (purple; representing the average of the west of the SIS domain), Dense Shelf Water (DSW) (light blue; representing the average of the modified Circumpolar Deep Water (mCDW) domain [65–66°S; 94–96°E]), and mCDW (red; representing the average of the mCDW domain) pertaining to the west of the SIS. The mCDW for the east of the SIS is shown in yellow. Historical data (diamond) are averaged over the period 1956–1996; seal data (circle) are averaged over the period 2004–2016. Lines over markers show one standard deviation. The black dots represent seal profiles (not averages) that fall into the region of the θ-S space corresponding to a three-point mixture between WW, ISW, and mCDW. The position of these profiles are shown as black dots on the map inset in (b). The three-point mixing generates a θ-S curve that has a linear portion between mCDW and the saltiest WW, and a curve that is close to the surface freezing point and extends from salty WW to fresh WW ("ideal" mixing line represented by the yellow thick line). The γ^n isopycnals of 27.7 (WW), 28 (mCDW), and 28.27 kg m^{-3} (DSW) are shown in gray in all panels. The horizontal black dotted line indicates the upper limit of DSW's temperature definition ($\theta = -1.8$°C). Seawater surface freezing point, which is also the lower limit of DSW's temperature definition to the right of the 28.27 kg m^{-3} isopycnal, is shown by the horizontal light blue dashed line.

$$\frac{d\theta}{dS} = \frac{L}{S_0 c_w} + \frac{(\theta_f - T_i)c_i}{S_0 c_w} + \frac{(\theta_0 - \theta_f)}{S_0} \quad (1)$$

where L is the latent heat of fusion for ice (3.35 × 105 J kg^{-1}); θ_0 and S_0 are the potential temperature and salinity, respectively, of the source water; c_w and c_i are the specific heat capacity of water and ice (4,000 and 2,010 J kg^{-1}°C^{-1}, respectively); and, θ_f is the potential freezing temperature at the ice shelf base. The slope of the line (α) for all lines drawn in this study is 2.6 and the temperature of the glacial ice (T_i) is −15°C (based on borehole temperatures reported from Mill Island and from the Amery Ice Shelf; Herraiz-Borreguero et al., 2013; Roberts et al., 2013). Two mixing lines are drawn (Figures 7a–7c) to determine if mCDW is causing basal melt of the SIS. If a water mass cools and freshens along the Gade line, it indicates mixing between glacial meltwater and the source water driving the melt. Two varieties of mCDW are used as end-members; a warmer ($\theta = -1.4$°C, $S = 34.46$) and a colder (−1.55°C, $S = 34.46$) variety.

No historical profiles fall along the Gade lines (Figure 7a). This is consistent with the absence of warm mCDW available to drive basal melt during that period (Figures 3a, 5c, 6a, and 6c). After 2004, the situation changes, with mCDW being able to reach the base of the ice shelf and melt it. This is shown by the cooling and freshening along the Gade line of, for example, mCDW with $\theta = -1.4$°C, and $S = 34.46$ (Figure 7b, black dashed line, red dots representing 4 out of 10 profiles from 2011), and mCDW with $\theta = -1.55$°C, $S = 34.46$ (Figure 7b, green dashed line, pink dots representing three profiles from 2014).

The warmest mCDW is found to the east of the SIS (Figure 7c), at the bottom of the profiles (not shown), where it has the potential to reach the deep grounding lines of the Denman and Scott Glaciers (ice shelf drafts ≈300 m; Brancato et al., 2020). While mCDW east of the SIS is 79.8 m thick, has an average potential temperature of -1.39 ± 0.32 and an average maximum potential temperature of -1.22 ± 0.38, the mCDW west of the SIS is 149.3 m thick, has an average potential temperature of -1.55 ± 0.25°C and an average maximum potential temperature of -1.53 ± 0.30°C. Nevertheless, the profiles in this data set do not lie on a Gade line connecting mCDW and meltwater (Figure 7c). To the east, data are averaged over the whole continental shelf, so historical data and seal data do not overlap spatially, particularly in the deep trough in front of the Denman Glacier. Thus, differences in spatial sampling could contribute to the differences we observe over time and conclusions for the east should be drawn with caution.

In Figure 7d, the time-mean values for each water mass are compared. To the west of the SIS, data for mCDW and DSW are averaged over the mCDW domain (red box; Figures 2b–2d), to ensure historical (diamonds) and seal data (circles) are overlapping. For ISW and WW, the west of the SIS domain is used. mCDW is warmer in the seal data than in the historical data. Dense Shelf Water (DSW) gets fresher with time, with seals recording the freshest values on average ($S = 34.47$) and a 0.06 decrease from the historical values. Like DSW, ISW has also become fresher. The magnitude of the salinity range for ISW is very large though, likely a result of multiple meltwater plumes exiting the cavity at different depths (Figure 5c), as demonstrated by melting occurring through two different Gade lines. Furthermore, although some profiles west of the SIS fit the proposed Gade lines (Figure 7b), we can't discard the possibility that other water masses, such as DSW and WW, are causing some of the observed melt, or that a 3-member mixture (mCDW, meltwater and WW) is at play.

Such mixing generates a θ-S curve that has a linear portion between mCDW and the saltiest WW, then a part of the curve that is close to the surface freezing point and extends from salty WW to fresh WW (represented by the yellow thick line in Figure 7d). In Figure 7d, we display five profiles, also from 2011 and in the vicinity of the SIS, that show this exact behavior in black dots. Although melting is present, when the melting process involves the mixture of three water masses, as opposed to two-point mixing of mCDW and meltwater, the θ/S points will not fall on the Gade lines.

Despite the observational evidence that mCDW is driving melt under the SIS in the seal data (Figure 7b, profiles along black and green Gade lines and Figure 7d, three-point mixing profiles), DSW is still present on the continental shelf during the same period. Given the historical data are limited to summer and early autumn, it is not possible to investigate the seasonal dependence of water mass changes observed between the historical and more recent period. However, in 2011 (Figure 8) the seal data cover most of the year with profiles showing that the warm mCDW present in summer and early autumn is largely eroded by cooling and deep convection in winter. In 2011, mCDW intrusions can be seen in the mid and bottom layers from February until April, with temperatures in the middle of the water column reaching −1°C in February. It is mostly eroded by June, with the majority of the water column made up of well-mixed profiles (Figure 8e). Then, winter convection starts and continues through the remaining months of available data, forming DSW (data points within the vertical dashed black lines). Up until May, all DSW in the shelf is remnant of the previous winter. Warm mCDW is back the following year (2012), occupying the middle of the shelf, but also reaching the tip of the SIS in August, with temperatures over −1°C below 500 m (not shown). The situation near the northern tip of the SIS is similar in 2013, although profiles are only available for March (not shown).

In 2014, although late autumn/winter data are not available to assess the onset of winter convection, warm mCDW intrusions are very strong during the months recorded by the seals (January-April; Figures 9a–9d) and the data distribution allows for comparison with the densest sampled year in the historical data (1966; Figures 9e–9g). The biologging data shows that mCDW is widespread on the shelf from January to April, both close to and distant from the SIS edge. In March, a layer with temperatures ranging between −1 and 0°C fills the water column between 300 and 600 dbar (Figure 9c). As a result, the mixed layer persists in April (Figure 9d) and is as shallow

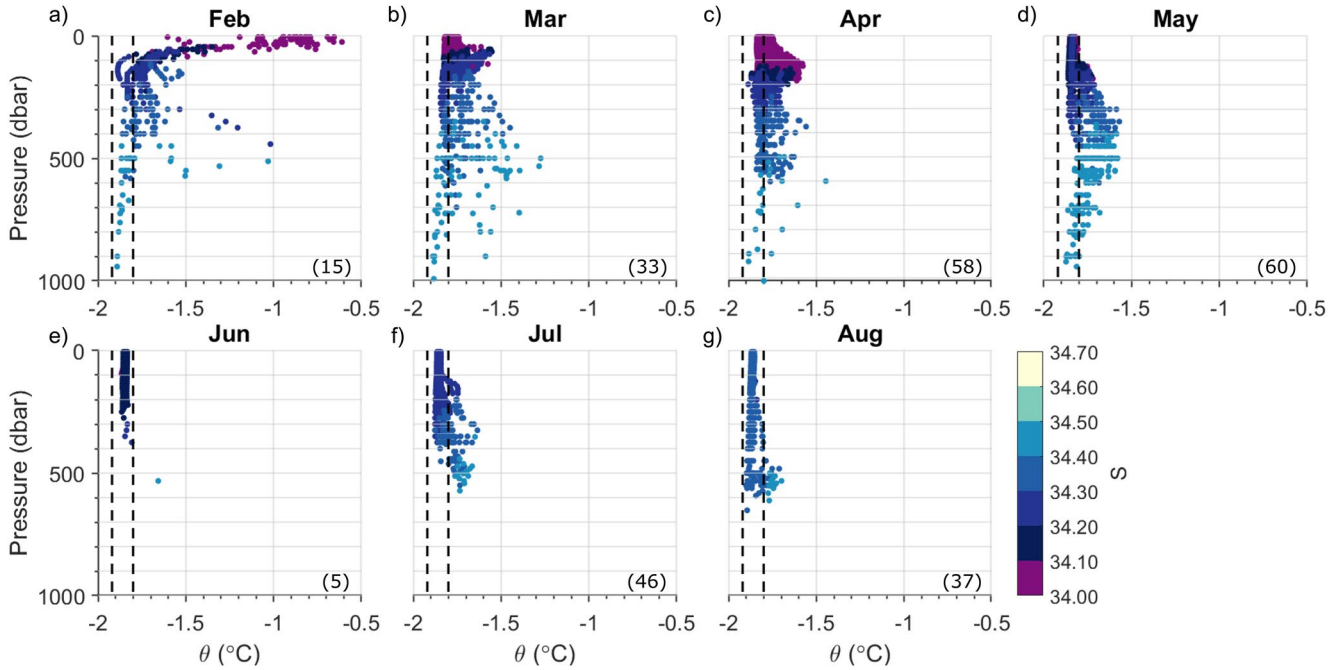

Figure 8. Seasonal evolution of vertical temperature and salinity profiles for the year of 2011 in the west of the Shackleton Ice Shelf domain. Data are displayed in vertical temperature profiles for each month available (a–g). Data are color-coded by salinity. Dashed black vertical lines correspond to the higher potential temperature limit of ISW's (−1.92°C) and DSW's (−1.8°C) definition. The number of profiles available for each month is displayed in the bottom right of each panel in between parenthesis.

as 100 m for all profiles available. In the historical profiles from about 50 years earlier, there is no record of these high temperatures in the shelf in mid or bottom layers. The contrast is also evident when salinity is considered, with waters with high salinity (>34.5) appearing at the bottom and as early as March (Figure 9f).

Overall, the seasonal variability of the most well sampled years (2011 and 2014) suggests that different water masses may access the ice shelf cavity at different times of year (i.e., warm mCDW in summer/autumn, cool DSW in winter). This was previously reported for the Amery Ice Shelf in Prydz Bay (Herraiz-Borreguero et al., 2015) and Vincennes Bay, where warm mCDW intrusions are eroded by heat loss in the polynya sometime after July (Ribeiro et al., 2021), allowing DSW to form and to reoccupy the deepest layers again. In 2011, mCDW in the Shackleton Polynya is eroded by June (Figure 8e), resulting in a late start to deep winter convection in relation to other parts of East Antarctica where DSW is formed, such as Adèlie Land (G. Williams et al., 2011) or the Mackenzie Polynya (Portela et al., 2022). Yet, winter convection starts earlier than in Vanderford Polynya, where no convection is observed until at least after July (Ribeiro et al., 2021).

4. Discussion

A comparison of recent profiles from southern elephant seals equipped with CTD-SRDL sensors (2004–2016) with historic ship-based measurements (1956–1996) shows that the shelf waters to the west of the Shackleton-Denman System have warmed because of the emergence of warmer mCDW intrusions (Figures 3a and 3d). These warm mCDW intrusions appear for the first time in the last 10 years of the 60-year time series (Figure 6c). Before 1996, warm mCDW was not observed as its temperature always remains below −1.6°C. However, since 2011, warm mCDW has been detected as it intrudes through two troughs west of the SIS, spreading to shallower depths on the continental shelf more broadly. This warming trend is also noticeable in the averaged thickness of WW for the west of the SIS, which is approximately halved in the biologging data set (43.9 m) compared to the historical data set (81.9 m). As mCDW is denser than WW, more frequent and longer intrusions increase the subsurface stratification and limit the depth of winter convection, decreasing WW thickness and depth. Conversely, in areas with less frequent or less intense mCDW intrusions, WW thickness may increase.

The warm mCDW observed since 2011 is driving basal melt of the SIS, and causing freshening of local DSW as indicated by θ/S profiles (Figure 7b). Data show warming of ISW but no significant change in its salinity.

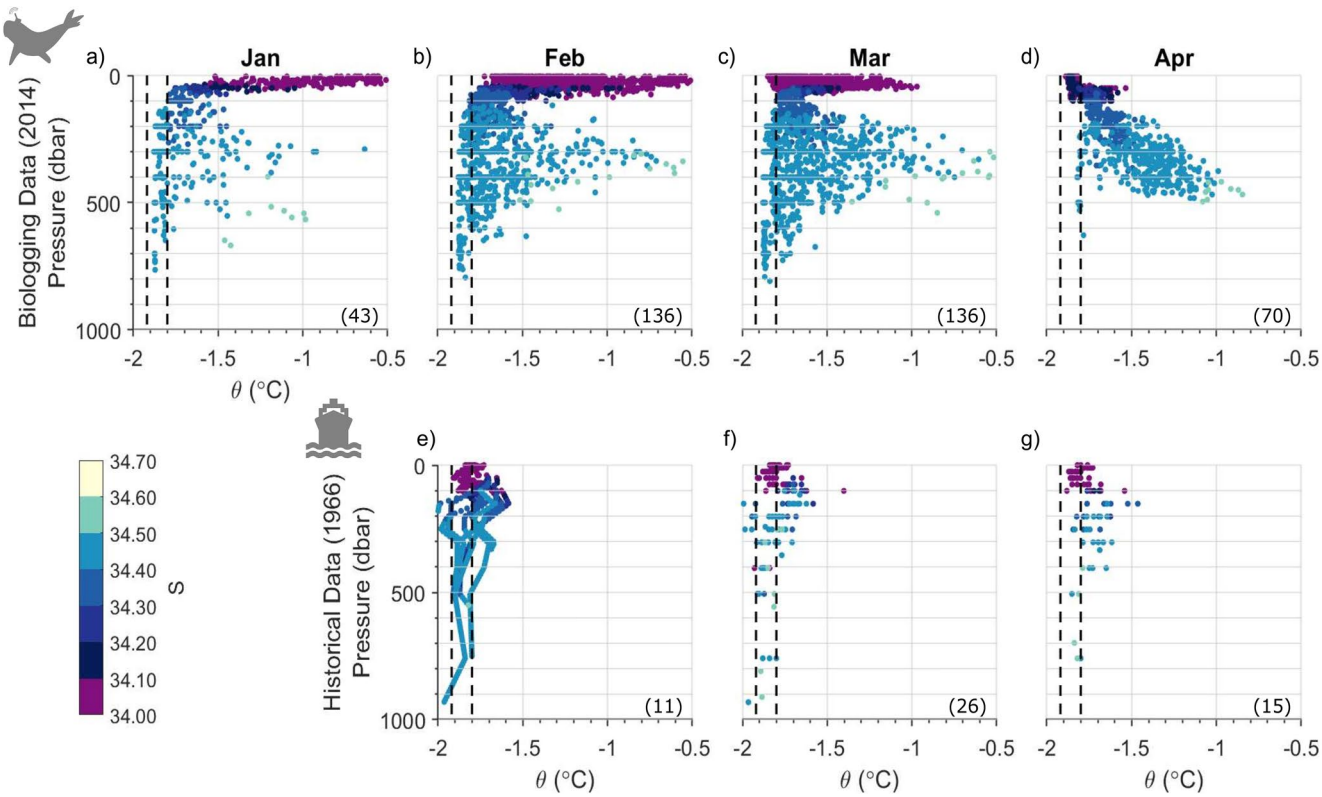

Figure 9. Seasonal evolution of vertical temperature and salinity profiles for the years of 2014 (a–d) and 1966 (e–g) in the west of the Shackleton Ice Shelf domain. Data are displayed in vertical temperature profiles for each month available. Data are color-coded by salinity. Dashed black vertical lines correspond to the higher potential temperature limit of ISW's (−1.92°C) and DSW's (−1.8°C) definition. The number of profiles available for each month is displayed in the bottom right of each panel in between parenthesis.

The wide range of salinity, however, indicates that different water masses drive basal melt at different times (Figure 7d). The depth layer occupied by ISW does not vary much between the two data sets, but it is thicker in the more recent seal data (inset of Figure 5c). Most of the historical data points are concentrated above 400 m, and only a single profile with warmer ISW reaches deeper, as can be seen when comparing the vertical distribution of ISW in both data sets (inset in Figure 5c). In contrast, the biologging data set has ISW data points that are somewhat evenly distributed across all layers between 0 and 700 dbar.

To the west of the SIS, warm mCDW intrusions were recorded for the first time near the ice shelf in 2011 and then in every year since. Intrusions reaching the Shackleton ice front are colder (mCDW $\theta_{max} = -1.2$°C) than those reaching the ice shelf front in other parts of East Antarctica (−0.5°C in Vincennes Bay (Ribeiro et al., 2021), −0.4°C on the Sabrina Coast (Rintoul et al., 2016) and 0.14°C in Lützow-Holm Bay (Hirano et al., 2020)). Nevertheless, they are still sufficiently warm to melt the SIS, reaching below the ice shelf draft (<300 m; Urbini et al., 2010) with temperatures up to 1°C above the local freezing point. This melt is also indicated by the θ/S profiles that fall on the Gade line in 2011 (Figure 7b) and the three-point mixing profile curves from 2011 (Figure 7d). The observations reveal warm water on the continental shelf during a time when the SIS experienced a thinning trend, losing approximately 1–2 m of ice each year between 1994 and 2012 (Paolo et al., 2015). Although we can only show melting from 2011 onwards, the warming of shelf waters may have started earlier but remained undetected given the more limited number of observations in the first years of the seal data series.

A possible consequence of the mCDW intrusions is the freshening of DSW. While the historical data set shows DSW with higher salinity values (>34.55) consistently occupying the whole continental shelf to the west of the SIS (Figure 3b), in the recent biologging data set, DSW only exceeds 34.55 near the shelf break (Figure 3e). When considering the west of the SIS domain, the average salinity of DSW is 0.06 higher than in the biologging data set (0.07 when only profiles within the DSW box are considered; Figures 2b–2d green box). Differences in maximum salinity values freshen by 0.1 in the latter as well. There are proportionally fewer DSW observations in the seal data and DSW is no longer the undisputed deepest water mass over the inner shelf, with mCDW now reaching similar

depths (Figures 4a and 4b). In fact, when compared to other DSW formation regions, the continental shelf west of the SIS is fresher, and the polynya struggles to form any DSW despite strong sea ice production (Portela et al., 2022).

The freshening of DSW has been recorded in other parts of the continental shelf in East Antarctica, and can be related to changes in polynya activity (Shadwick et al., 2013) or to the basal melt of local ice shelves (Silvano et al., 2018). In the Mertz Polynya, the calving of the Mertz Glacier Tongue changed the polynya configuration, reducing its sea ice production and, hence, the salinity of DSW (Shadwick et al., 2013). Modeling work along the Totten Glacier showed that freshwater input from ice shelf melting was enough to offset the salt flux from sea ice production, preventing top-to-bottom convection (Silvano et al., 2018). Given there were no significant changes in the icescape of the Shackleton-Denman System in the last 60 years (S. S. Thompson et al., 2023) or in the activity of the Shackleton Polynya (sea ice production increases 0.09% per year from 1992 to 2013; Tamura et al., 2016), it seems the freshening of DSW is more likely the result of melting (and thinning; Paolo et al., 2015) of the SIS.

The ISW characteristics in the area are also an indication that the basal melt process for the SIS is not always a simple two-point mixing between end-members with fixed properties as shown in Figure 7b, but rather involves different water masses (DSW, mCDW, and WW) generating different types of meltwater. The biologging data set shows a cluster of ISW with minimum temperatures 0.02–0.03°C higher than any ISW recorded in the historical data set (Figure 3c) occupying a wide range of depth (Figure 4b and inset in Figure 5c). These warmer temperatures suggest the melting is either by warm mCDW at shallow depths, or by both mCDW and DSW at the bottom at different times of the year. This further indicates there is an alternation between warm- and cold-shelf modes in the SIS, instead of a continuously mCDW-flooded continental shelf, as found in West Antarctica (e.g., Jacobs et al., 2011; Silvano et al., 2016).

The evidence suggests mCDW intrusions cause two different modes of basal melting in the SIS: (a) a two-point mixing basal melt, where mCDW causes basal melt, and a (b) three-point mixing process, when both mCDW and WW interact and cause basal melt. In the latter, the mixture of mCDW and glacial meltwater, which may or may not be cold enough to be classified as ISW, ascends along the base of the ice shelf, mixing with WW and then exiting the ice shelf cavity. In Vincennes Bay, where much warmer mCDW intrusions occurred in 2012, two-point mixing basal melt was also observed (Ribeiro et al., 2021). The three-point mixing process was reported in the Totten Glacier, where the shelf is fresher than in Vincennes Bay (Silvano et al., 2017).

The schematic in Figure 10 summarizes the main findings. We suggest that the continental shelf adjacent to the SIS has shifted from a cold mode (Figure 10a), where DSW is the densest water mass on the shelf, to a warm mode (Figure 10b), where primarily mid-depth (warmer; up to −1.0°C) and occasionally bottom mCDW intrusions (<−1.4°C) reach the shelf. In the cold shelf mode, sea ice formation and the loss of heat through the polynyas lead to winter convection and DSW formation, which can enter the ice shelf cavity and drive basal melt (Figure 10a). In the warm mode, mCDW occupies mid and deep layers, reaching the ice shelf and causing basal melt of the SIS (Figure 10b). Glacial melt may mix with mCDW and exit the cavity without mixing with other waters (Figure 10b(1)), or the meltwater produced by mCDW reaching the ice shelf (Figure 10b(2a)) may mix with WW as it ascends before exiting the cavity (Figure 10b(2b)). mCDW intrusions delay the onset of winter convection by increasing stratification of the water column through enhanced basal melt (Silvano et al., 2017) and by bringing more heat into the system, which hinders (Figure 10(3)) DSW formation (Ribeiro et al., 2021). Albeit delayed, once mCDW is eroded by polynya activity, the winter convection can reach the bottom and start forming DSW, with the shelf waters reverting to the cold mode (Figure 10(4)). Reduced amounts of DSW remnant from the previous winter (Figure 8) also sit at the bottom in some areas of the polynya (Figure 10b).

The seal-derived data used in our study are unevenly distributed in time and space on the shelf, so that differences between data sets might reflect spatial or temporal aliasing. To minimize aliasing, we only compared observations from the same area and season. Along the same lines, although seals may exhibit preferences in terms of their foraging behaviors in the ocean (e.g., polynyas; Arce et al., 2022; Labrousse et al., 2018), there is evidence showing that water temperature is not an influential variable when determining habitat selection in post-molt elephant seals. In fact, the relationship between temperature and seal foraging was shown to be negative (i.e., seals selected areas with cold water more than areas with warm water Hindell et al., 2020). Consequently, it is unlikely that the observed increases in temperature are a result of seals specifically choosing areas with disproportionately warmer waters, thereby suggesting that significant biases in the observations are improbable.

The mechanisms driving mCDW intrusions onto the continental shelves in Antarctica is a topic of intense debate. Remote factors, such as changes in ocean gyres (Yamazaki et al., 2021), eddy fields (e.g., Totten Ice Shelf; Hirano

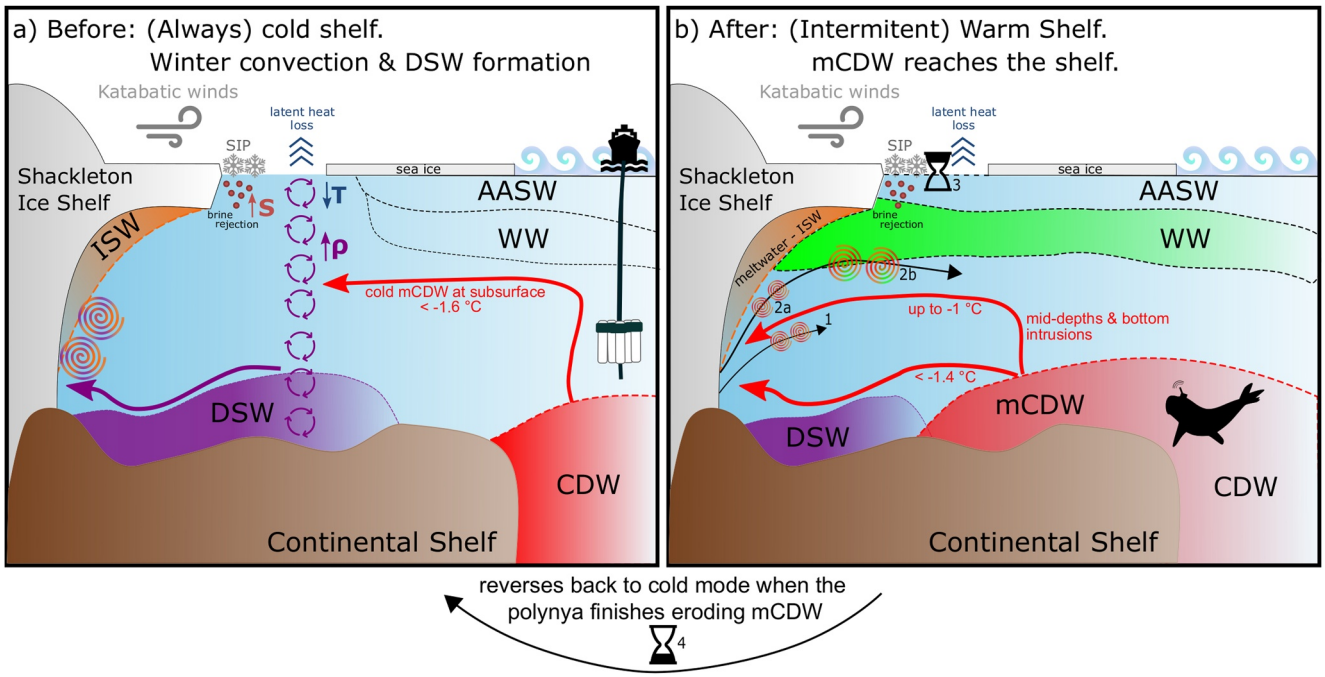

Figure 10. Seasonal shift in the continental shelf oceanography and ocean/ice shelf interactions for summer/autumn in the Shackleton Ice Shelf (SIS). (a) The historical data show that continental shelf waters west of the SIS were cold. Here, winter convection starts in early autumn and forms relatively saline Dense Shelf Water (DSW). Cold DSW, as the densest water mass on the shelf, reaches the grounding line and drives relatively low rates of basal melt. AASW/WW may also penetrate below the ice shelf and drive melt at shallower depths. Only very cold modified Circumpolar Deep Water (mCDW) was present ($\theta < -1.6$°C) and limited to the subsurface. (b) The biologging data set shows a shift to a warm shelf, where mCDW has largely replaced DSW. The presence of mCDW delays the start of winter convection, so DSW formation is inhibited. Remnant DSW trapped from the previous winter sits at the bottom in some areas of the polynya, but the distribution is limited. Here, data suggest melting by mCDW generates two varieties of meltwater mixtures: (1) two-point mixing between mCDW and ice melt forms Ice Shelf Water, with a range of salinities reflecting the salinity of the mCDW driving melt, and (2) three-point mixing when mCDW and glacial water mix with WW. In this case, mCDW drives melt (2a) at depth or mid-depth and the mixture of mCDW and meltwater ascends, mixing with WW before exiting the cavity (2b). Brine rejected by sea ice formation in the polynya erodes mCDW and eventually winter convection begins (3), with the shelf stratification returning to the cold mode (4). However, the delayed start of the convection reduces the salinity of the DSW formed. The indicated temperature values for mCDW consider the mCDW domain (red box in Figures 2 and 5). Water masses are not depicted to scale in terms of their average thickness, and the schematic does not accurately represent their precise depth distribution.

et al., 2021) and the southern displacement of zonal winds (Herraiz-Borreguero & Naveira Garabato, 2022) may contribute. In addition, local factors, such as variability in the Antarctic Slope Current (e.g., Totten Ice Shelf; Nakayama et al., 2021), coastal Ekman pumping (Spence et al., 2014), and Ekman pumping along the slope (e.g., Totten Ice Shelf; Greene et al., 2017), among others, may play a role, with the relative importance of different mechanisms varying from one region to another. Although it is still unclear how mCDW reaches the continental shelves in the SIS area, Herraiz-Borreguero and Naveira Garabato (2022) showed warming of 2–3°C within the CDW layer in the continental slope, which implies a direct increase in the ocean heat supply available to melt the Shackleton-Denman system. The observed oceanographic changes within Vincennes Bay further support this study's documented changes, with mCDW replacing DSW at the bottom of the water column in front of the Vanderford Glacier (Herraiz-Borreguero & Naveira Garabato, 2022; Ribeiro et al., 2021).

The east of the SIS, including the Denman Glacier, is also experiencing inflow of warm mCDW, similar to the west of the SIS. Recent studies using Argo floats (van Wijk et al., 2022) have observed strong heat transport into the Denman Glacier cavity, and two seal profiles presented in this study show warm mCDW at the bottom layer reaching its calving front. Unfortunately, there is not enough historical data to assess how the conditions have changed on that side over time. However, if such a shift did occur to the east of the SIS, it might explain the grounding line retreat and flow acceleration of the Denman Glacier observed between 1996 and 2018 (Brancato et al., 2020).

5. Conclusions

The vulnerability of the East Antarctic continental shelf to warm mCDW remains poorly understood, and little is known about how this exposure has changed over the years due to the general lack of historical data in the

region. In that regard, the region west of the SIS, where oceanographic measurements span 60 years from 1956 to 2016, is an exception, providing the possibility of investigating temporal changes. Our examination of this data set shows that in the last decade the region is subject to an increase of warmer mCDW intrusions. Whereas previously the mCDW on the shelf was cooler and limited in its influence and extent, from 2011 the mCDW is observed to be much warmer and widespread across the continental shelf, extending to the ice front of the SIS, which is in line with the observed warming of the CDW layer over the continental slope (Herraiz-Borreguero & Naveira Garabato, 2022).

More warm water is reaching the continental shelf in the Shackleton-Denman System and threatening the SIS. The observed intrusions can lead to increased basal melt under the SIS, and, then, the increase in freshwater supply can hinder the production of DSW (Herraiz-Borreguero & Naveira Garabato, 2022; Ribeiro et al., 2021; Silvano et al., 2017; G. D. Williams et al., 2016) and allow for more mCDW intrusions (Silvano et al., 2017). These intrusions can potentially access the ice shelf cavity and enhance basal melting. The results of this study show that warm mCDW reaches the ice front on both the eastern and western sides of the SIS and highlight the potential sensitivity of the SIS to future warming.

While the Shackleton-Denman System has received increased attention following observations of thinning (Paolo et al., 2015), large meltwater input (van Wijk et al., 2022), and grounding line retreat (Brancato et al., 2020), the dynamics of the area are far from being fully understood and the drivers of increased mCDW intrusions in the region are still unknown. Given the potential instability of the Denman Glacier, which sits on a retrograde bed (Morlighem et al., 2020), it is important to continue to monitor changes in the region and to understand what drives the variability of its dynamic processes, both in the past and in the future. Biologging data and other ocean sampling technologies, such as Argo floats (McMahon et al., 2021; Notarstefano, 2022), have allowed the scientific community to make more observations of the Antarctic continental shelves than ever before. Continuing to build on these sampling capabilities will enhance our understanding of the vulnerability of the EAIS to changes in the surrounding ocean and the potential impact on future sea-level rise.

Data Availability Statement

The historical data used in this study were extracted from the Southern Ocean Data Base (SODB; described in Orsi & Whitworth, 2005, https://zenodo.org/record/4071923#.YkKx1ChBw2w), World Ocean Atlas (WOA; versions prior to 2003; https://www.ncei.noaa.gov/products/world-ocean-atlas), and WOCE Global Hydrographic Climatology (WOCE; https://odv.awi.de/data/ocean/woce-global-hydrographic-climatology/) and are free and publicly available. The biologging data set used in this study are described in Treasure et al. (2017); Roquet et al. (2014, 2017). Data are open access and can be found at the MEOP consortium website https://www.meop.net/database/meop-databases/density-of-data.html and access to it may be requested by filling in this form https://www.meop.net/download2/. All Matlab code that has been developed to create figures for this manuscript has been uploaded to a public GitHub repository that can be accessed through this link https://github.com/ribeiron/Oceanic_regime_shift_paper_2023_code_library. Minor alterations were sometimes done using Inkscape, but the code is sufficient to reproduce the data as shown in this document.

Acknowledgments
This project and authors received grant funding from the University of Tasmania, the Australian Research Council (DP180101667), and the Australian Government as part of the Antarctic Science Collaboration Initiative program (ASCI00002) and by the Centre for Southern Hemisphere Oceans Research, a collaboration between CSIRO, the Qingdao National Laboratory for Marine Science and Technology (QNLM), the University of Tasmania and the University of New South Wales. The seal CTD-SRDL tags and deployment were funded and supported through a collaboration between the French Polar Institute (program 109: PI. H. Weimerskirch and 1201: PI. C. Gilbert and C. Guinet), the SNO-MEMO and CNES-TOSCA and the Integrated Marine Observing System (IMOS). IMOS is enabled by the National Collaborative Research Infrastructure Strategy (NCRIS) and is operated by a consortium of institutions as an unincorporated joint venture, with the University of Tasmania as Lead Agent. The authors would like to thank the MEOP consortium and all scientists who participated in the data collection and processing of the Southern Ocean Data Base (SODB), World Ocean Atlas (WOA), and WOCE Global Hydrographic Climatology (WOCE), making all data used in this work free and publicly available. We would like to thank Dr. Sarah Thompson and Dr. Roland Warner from UTAS for their advice regarding reviewers' glaciological enquiries, and Ms Esmee van Wijk for her support on the enquiries regarding the east of the Shackleton Ice Shelf, during the peer-review process of this manuscript. Finally, we would also like to thank and acknowledge Dr. Kaihe Yamazaki and the anonymous reviewers for their thorough, thoughtful and positive reviews of our paper. Our paper has been improved greatly by their input. Open access publishing facilitated by University of Tasmania, as part of the Wiley - University of Tasmania agreement via the Council of Australian University Librarians.

References

Abraham, J. P., Gorman, J., Reseghetti, F., Sparrow, E. M., & Minkowycz, W. (2012). Drag coefficients for rotating expendable bathythermographs and the impact of launch parameters on depth predictions. *Numerical Heat Transfer, Part A: Applications*, *62*(1), 25–43. https://doi.org/10.1080/10407782.2012.672898

Adusumilli, S., Fricker, H. A., Medley, B., Padman, L., & Siegfried, M. R. (2020). Interannual variations in meltwater input to the Southern Ocean from Antarctic ice shelves. *Nature Geoscience*, *13*(9), 616–620. https://doi.org/10.1038/s41561-020-0616-z

Arce, F., Hindell, M. A., McMahon, C. R., Wotherspoon, S. J., Guinet, C., Harcourt, R. G., & Bestley, S. (2022). Elephant seal foraging success is enhanced in Antarctic coastal polynyas. *Proceedings of the Royal Society B*, *289*(1967), 20212452. https://doi.org/10.1098/rspb.2021.2452

Brancato, V., Rignot, E., Milillo, P., Morlighem, M., Mouginot, J., An, L., et al. (2020). Grounding line retreat of Denman Glacier, East Antarctica, measured with COSMO-SkyMed radar interferometry data. *Geophysical Research Letters*, *47*(7), e2019GL086291. https://doi.org/10.1029/2019gl086291

Brown, N. L., & Hamon, B. V. (1961). An inductive salinometer. *Deep-Sea Research*, *8*(1), 65-IN. https://doi.org/10.1016/0146-6313(61)90015-6

Edwards, T. L., Brandon, M. A., Durand, G., Edwards, N. R., Golledge, N. R., Holden, P. B., et al. (2019). Revisiting Antarctic ice loss due to marine ice-cliff instability. *Nature*, *566*(7742), 58–64. https://doi.org/10.1038/s41586-019-0901-4

Foldvik, A., & Kvinge, T. (1974). Conditional instability of sea water at the freezing point. In *Deep sea research and oceanographic abstracts* (Vol. 21, pp. 169–174). Elsevier.

Fraser, A. D., Massom, R. A., Handcock, M. S., Reid, P., Ohshima, K. I., Raphael, M. N., et al. (2021). Eighteen-year record of circum-antarctic landfast-sea-ice distribution allows detailed baseline characterisation and reveals trends and variability. *The Cryosphere*, *15*(11), 5061–5077. https://doi.org/10.5194/tc-15-5061-2021

Fretwell, P., Pritchard, H. D., Vaughan, D. G., Bamber, J. L., Barrand, N. E., Bell, R., et al. (2013). Bedmap2: Improved ice bed, surface and thickness datasets for Antarctica. *The Cryosphere*, *7*(1), 375–393. https://doi.org/10.5194/tc-7-375-2013

Gade, H. G. (1979). Melting of ice in sea water: A primitive model with application to the Antarctic ice shelf and icebergs. *Journal of Physical Oceanography*, *9*(1), 189–198. https://doi.org/10.1175/1520-0485(1979)009<0189:moiisw>2.0.co;2

Gille, S. T., McKee, D. C., & Martinson, D. G. (2016). Temporal changes in the Antarctic circumpolar current: Implications for the Antarctic continental shelves. *Oceanography*, *29*(4), 96–105. https://doi.org/10.5670/oceanog.2016.102

Gouretski, V., & Reseghetti, F. (2010). On depth and temperature biases in bathythermograph data: Development of a new correction scheme based on analysis of a global ocean database. *Deep Sea Research Part I: Oceanographic Research Papers*, *57*(6), 812–833. https://doi.org/10.1016/j.dsr.2010.03.011

Greene, C. A., Blankenship, D. D., Gwyther, D. E., Silvano, A., & van Wijk, E. (2017). Wind causes Totten ice shelf melt and acceleration. *Science Advances*, *3*(11), e1701681. https://doi.org/10.1126/sciadv.1701681

Harcourt, R., Sequeira, A. M. M., Zhang, X., Roquet, F., Komatsu, K., Heupel, M., et al. (2019). Animal-Borne telemetry: An integral component of the ocean observing toolkit. *Frontiers in Marine Science*, *6*, 326. https://doi.org/10.3389/fmars.2019.00326

Herraiz-Borreguero, L., Allison, I., Craven, M., Nicholls, K. W., & Rosenberg, M. A. (2013). Ice shelf/ocean interactions under the Amery Ice Shelf: Seasonal variability and its effect on marine ice formation. *Journal of Geophysical Research: Oceans*, *118*(12), 7117–7131. https://doi.org/10.1002/2013jc009158

Herraiz-Borreguero, L., Church, J. A., Allison, I., Peña-Molino, B., Coleman, R., Tomczak, M., & Craven, M. (2016). Basal melt, seasonal water mass transformation, ocean current variability, and deep convection processes along the Amery Ice Shelf calving front, East Antarctica. *Journal of Geophysical Research: Oceans*, *121*(7), 4946–4965. https://doi.org/10.1002/2016jc011858

Herraiz-Borreguero, L., Coleman, R., Allison, I., Rintoul, S. R., Craven, M., & Williams, G. D. (2015). Circulation of modified circumpolar deep water and basal melt beneath the Amery Ice Shelf, East Antarctic. *Journal of Geophysical Research: Oceans*, *120*(4), 3098–3112. https://doi.org/10.1002/2015jc010697

Herraiz-Borreguero, L., & Naveira Garabato, A. C. (2022). Poleward shift of circumpolar deep water threatens the East Antarctic Ice Sheet. *Nature Climate Change*, *12*(8), 1–7. https://doi.org/10.1038/s41558-022-01424-3

Hindell, M. A., Reisinger, R. R., Ropert-Coudert, Y., Hückstädt, L. A., Trathan, P. N., Bornemann, H., et al. (2020). Tracking of marine predators to protect Southern Ocean ecosystems. *Nature*, *580*(7801), 87–92. https://doi.org/10.1038/s41586-020-2126-y

Hirano, D., Mizobata, K., Sasaki, H., Murase, H., Tamura, T., & Aoki, S. (2021). Poleward eddy-induced warm water transport across a shelf break off Totten Ice Shelf, East Antarctica. *Communications Earth Environment*, *2*(1), 1–8. https://doi.org/10.1038/s43247-021-00217-4

Hirano, D., Tamura, T., Kusahara, K., Ohshima, K. I., Nicholls, K. W., Ushio, S., et al. (2020). Strong ice-ocean interaction beneath Shirase Glacier Tongue in East Antarctica. *Nature Communications*, *11*(1), 1–12. https://doi.org/10.1038/s41467-020-17527-4

Jacobs, S., Jenkins, A., Giulivi, C. F., & Dutrieux, P. (2011). Stronger ocean circulation and increased melting under Pine Island Glacier ice shelf. *Nature Geoscience*, *4*(8), 519–523. https://doi.org/10.1038/ngeo1188

Jenkins, A. (1999). The impact of melting ice on ocean waters. *Journal of Physical Oceanography*, *29*(9), 2370–2381. https://doi.org/10.1175/1520-0485(1999)029<2370:tiomio>2.0.co;2

Jonsen, I. D., Patterson, T. A., Costa, D. P., Doherty, P. D., Godley, B. J., Grecian, W. J., et al. (2020). A continuous-time state-space model for rapid quality-control of Argos locations from animal-borne tags. *Movement Ecology*, *8*(1), 31. https://doi.org/10.1186/s40462-020-00217-7

Labrousse, S., Williams, G., Tamura, T., Bestley, S., Sallée, J.-B., Fraser, A. D., et al. (2018). Coastal polynyas: Winter oases for subadult southern elephant seals in East Antarctica. *Scientific Reports*, *8*(1), 1–15. https://doi.org/10.1038/s41598-018-21388-9

McMahon, C. R., Hindell, M. A., Charrassin, J. B., Coleman, R., Guinet, C., Harcourt, R., et al. (2023). Southern Ocean pinnipeds provide bathymetric insights on the East Antarctic continental shelf. *Communications Earth & Environment*, *4*(1), 266. https://doi.org/10.1038/s43247-023-00928-w

McMahon, C. R., Roquet, F., Baudel, S., Belbeoch, M., Bestley, S., Blight, C., et al. (2021). Animal borne ocean sensors-AniBOS—An essential component of the global ocean observing system (GOOS). *Frontiers in Marine Science*, *18*, 751840. https://doi.org/10.3389/fmars.2021.751840

Mensah, V., Roquet, F., Siegelman-Charbit, L., Picard, B., Pauthenet, E., & Guinet, C. (2018). A correction for the thermal mass–induced errors of CTD tags mounted on marine mammals. *Journal of Atmospheric and Oceanic Technology*, *35*(6), 1237–1252. https://doi.org/10.1175/jtech-d-17-0141.1

Morlighem, M., Rignot, E., Binder, T., Blankenship, D., Drews, R., Eagles, G., et al. (2020). Deep glacial troughs and stabilizing ridges unveiled beneath the margins of the Antarctic ice sheet. *Nature Geoscience*, *13*(2), 132–137. https://doi.org/10.1038/s41561-019-0510-8

Nakayama, Y., Greene, C. A., Paolo, F. S., Mensah, V., Zhang, H., Kashiwase, H., et al. (2021). Antarctic slope current modulates ocean heat intrusions towards Totten Glacier. *Geophysical Research Letters*, *48*(17), e2021GL094149. https://doi.org/10.1029/2021gl094149

Nicholls, K. W., Østerhus, S., Makinson, K., Gammelsrød, T., & Fahrbach, E. (2009). Ice-ocean processes over the continental shelf of the southern Weddell Sea, Antarctica: A review. *Reviews of Geophysics*, *47*(3), RG3003. https://doi.org/10.1029/2007rg000250

Notarstefano, G. (2022). Argo float data and metadata from global data Assembly centre (Argo GDAC) [Dataset]. SEANOE. https://doi.org/10.17882/42182

Orsi, A. H., & Whitworth, T. (2005). *Hydrographic atlas of the World Ocean circulation Experiment (WOCE): Volume 1: Southern Ocean*. WOCE International Project Office Southampton.

Paolo, F. S., Fricker, H. A., & Padman, L. (2015). Volume loss from Antarctic ice shelves is accelerating. *Science*, *348*(6232), 327–331. https://doi.org/10.1126/science.aaa0940

Portela, E., Rintoul, S. R., Herraiz-Borreguero, L., Roquet, F., Bestley, S., Van Wijk, E., et al. (2022). Controls on dense shelf water formation in four East Antarctic polynyas. *Journal of Geophysical Research: Oceans*, *127*(12), e2022JC018804. https://doi.org/10.1029/2022jc018804

Pritchard, H., Ligtenberg, S. R., Fricker, H. A., Vaughan, D. G., van den Broeke, M. R., & Padman, L. (2012). Antarctic ice-sheet loss driven by basal melting of ice shelves. *Nature*, *484*(7395), 502–505. https://doi.org/10.1038/nature10968

Ribeiro, N., Herraiz-Borreguero, L., Rintoul, S., McMahon, C., Hindell, M., Harcourt, R., & Williams, G. (2021). Warm modified circumpolar deep water intrusions drive ice shelf melt and inhibit dense shelf water formation in Vincennes Bay, East Antarctica. *Journal of Geophysical Research: Oceans*, *126*(8), e2020JC016998. https://doi.org/10.1029/2020jc016998

Rignot, E., Jacobs, S., Mouginot, J., & Scheuchl, B. (2013). Ice-shelf melting around Antarctica. *Science*, *341*(6143), 266–270. https://doi.org/10.1126/science.1235798

Rignot, E., Mouginot, J., Scheuchl, B., Van Den Broeke, M., Van Wessem, M. J., & Morlighem, M. (2019). Four decades of Antarctic ice sheet mass balance from 1979–2017. *Proceedings of the National Academy of Sciences*, *116*(4), 1095–1103. https://doi.org/10.1073/pnas.1812883116

Rintoul, S. R., Silvano, A., Pena-Molino, B., van Wijk, E., Rosenberg, M., Greenbaum, J. S., & Blankenship, D. D. (2016). Ocean heat drives rapid basal melt of the Totten Ice Shelf. *Science Advances*, *2*(12), e1601610. https://doi.org/10.1126/sciadv.1601610

Roberts, J., Moy, A., Van Ommen, T., Curran, M., Worby, A., Goodwin, I., & Inoue, M. (2013). Borehole temperatures reveal a changed energy budget at Mill Island, East Antarctica, over recent decades. *The Cryosphere*, *7*(1), 263–273. https://doi.org/10.5194/tc-7-263-2013

Roquet, F., Boehme, L., Block, B., Charrasin, J. B., Costa, D., Guinet, C., et al. (2017). Ocean observations using tagged animals. *Oceanography*, *30*(2), 139. https://doi.org/10.5670/oceanog.2017.235

Roquet, F., Williams, G., Hindell, M. A., Harcourt, R., McMahon, C., Guinet, C., et al. (2014). A Southern Indian Ocean database of hydrographic profiles obtained with instrumented elephant seals. *Scientific Data*, *1*, 140028. https://doi.org/10.1038/sdata.2014.28

Shadwick, E., Rintoul, S. R., Tilbrook, B., Williams, G., Young, N., Fraser, A., et al. (2013). Glacier tongue calving reduced dense water formation and enhanced carbon uptake. *Geophysical Research Letters*, *40*(5), 904–909. https://doi.org/10.1002/grl.50178

Siegelman, L., Roquet, F., Mensah, V., Rivière, P., Pauthenet, E., Picard, B., & Guinet, C. (2019). Correction and accuracy of high-and low-resolution CTD data from animal-borne instruments. *Journal of Atmospheric and Oceanic Technology*, *36*(5), 745–760. https://doi.org/10.1175/jtech-d-18-0170.1

Silvano, A., Rintoul, S., & Herraiz-Borreguero, L. (2016). Ocean-ice shelf interaction in East Antarctica. *Oceanography*, *29*(4), 130–143. https://doi.org/10.5670/oceanog.2016.105

Silvano, A., Rintoul, S. R., Peña-Molino, B., Hobbs, W. R., van Wijk, E., Aoki, S., et al. (2018). Freshening by glacial meltwater enhances melting of ice shelves and reduces formation of Antarctic Bottom Water. *Science Advances*, *4*(4), eaap9467. https://doi.org/10.1126/sciadv.aap9467

Silvano, A., Rintoul, S. R., Peña-Molino, B., & Williams, G. D. (2017). Distribution of water masses and meltwater on the continental shelf near the Totten and Moscow University ice shelves. *Journal of Geophysical Research: Oceans*, *122*(3), 2050–2068. https://doi.org/10.1002/2016JC012115

Smith, B., Fricker, H. A., Gardner, A. S., Medley, B., Nilsson, J., Paolo, F. S., et al. (2020). Pervasive ice sheet mass loss reflects competing ocean and atmosphere processes. *Science*, *368*(6496), 1239–1242. https://doi.org/10.1126/science.aaz5845

Spence, P., Griffies, S. M., England, M. H., Hogg, A. M., Saenko, O. A., & Jourdain, N. C. (2014). Rapid subsurface warming and circulation changes of Antarctic coastal waters by poleward shifting winds. *Geophysical Research Letters*, *41*(13), 4601–4610. https://doi.org/10.1002/2014GL060613

Tamura, T., Ohshima, K. I., Fraser, A. D., & Williams, G. D. (2016). Sea ice production variability in Antarctic coastal polynyas. *Journal of Geophysical Research: Oceans*, *121*(5), 2967–2979. https://doi.org/10.1002/2015jc011537

Thompson, A. F., Stewart, A. L., Spence, P., & Heywood, K. J. (2018). The Antarctic slope current in a changing climate. *Reviews of Geophysics*, *56*(4), 741–770. https://doi.org/10.1029/2018RG000624

Thompson, S. S., Kulessa, B., Luckman, A., Halpin, J. A., Greenbaum, J. S., Pelle, T., et al. (2023). Glaciological history and structural evolution of the Shackleton ice shelf system, East Antarctica, over the past 60 years. *The Cryosphere*, *17*(1), 157–174. https://doi.org/10.5194/tc-17-157-2023

Thomson, R. E., & Emery, W. J. (2014). *Data analysis methods in physical oceanography*. Newnes.

Treasure, A. M., Roquet, F., Ansorge, I. J., Bester, M. N., Boehme, L., Bornemann, H., et al. (2017). Marine mammals exploring the Oceans pole to pole: A review of the MEOP consortium [Dataset]. Oceanography, *30*(2), 132–138. https://doi.org/10.5670/oceanog.2017.234

Urbini, S., Cafarella, L., Zirizzotti, A., Tabacco, I. E., Bottari, C., Baskaradas, J. A., & Neal Young (2010). Radio echo sounding data analysis of the Shackleton Ice Shelf. *Annals of Geophysics*, *53*(2), 79–87. https://doi.org/10.4401/ag-4563

van Wijk, E. M., Rintoul, S. R., Wallace, L. O., Ribeiro, N., & Herraiz-Borreguero, L. (2022). Vulnerability of Denman Glacier to ocean heat flux revealed by profiling float observations. *Geophysical Research Letters*, *49*, e2022GL100460. https://doi.org/10.1029/2022GL100460

Whitworth, T., Orsi, A., Kim, S., Nowlin, W., Locarnini, R., Jacobs, S., & Weiss, R. (1998). Ocean, ice, and atmosphere: Interactions at the Antarctic continental margin. In S. S. Jacobs & R. F. Weiss (Eds.), *Antarctic research series* (Vol. 75, pp. 1–28).

Williams, G., Meijers, A. J. S., Poole, A., Mathiot, P., Tamura, T., & Klocker, A. (2011). Late winter oceanography off the Sabrina and BANZARE coast (117–128°E), East Antarctica. *Deep Sea Research Part II: Topical Studies in Oceanography*, *58*(9–10), 1194–1210. https://doi.org/10.1016/j.dsr2.2010.10.035

Williams, G. D., Herraiz-Borreguero, L., Roquet, F., Tamura, T., Ohshima, K. I., Fukamachi, Y., et al. (2016). The suppression of Antarctic Bottom Water formation by melting ice shelves in Prydz Bay. *Nature Communications*, *7*(1), 12577. https://doi.org/10.1038/ncomms12577

Yamazaki, K., Aoki, S., Katsumata, K., Hirano, D., & Nakayama, Y. (2021). Multidecadal poleward shift of the southern boundary of the Antarctic circumpolar current off East Antarctica. *Science Advances*, *7*(24), eabf8755. https://doi.org/10.1126/sciadv.abf8755

Yamazaki, K., Aoki, S., Shimada, K., Kobayashi, T., & Kitade, Y. (2020). Structure of the Subpolar Gyre in the Australian-Antarctic basin derived from Argo floats. *Journal of Geophysical Research: Oceans*, *125*(8), e2019JC015406. https://doi.org/10.1029/2019JC015406